UNIVERSITAT POLITÈCNICA DE CATALUNYA
BARCELONATECH
Departament de Teoria del Senyal
i Comunicacions

Performance Evaluation of an Interference Cancellation Scheme for the Uplink of a Massive User Network

A Master's Thesis Submitted to the Faculty of the
Escola Tècnica Superior d'Enginyeria de Telecomunicació de Barcelona
Universitat Politècnica de Catalunya

Author:
Francesc Molina Oliveras

In partial fulfilment of the requirements for the degree of
MASTER IN TELECOMMUNICATIONS ENGINEERING

Advisors:
Josep Sala Álvarez
Javier Villares Piera

Signal Processing and Communications Group
Department of Signal Theory and Communications

Barcelona, July 2017

Abstract

Inter-user interference constitutes a limiting factor to network performance, especially when dense wireless systems sustaining high traffic loads are deployed. Interference cancellation (IC) policies have proved an invaluable tool in order to counteract this problem. Nonetheless, the success of such IC schemes depends heavily on the received power distribution. In this work, we consider a massive user spread-spectrum Multiple Access (MA) network for wide area Machine to Machine (M2M) communications in which the central node implements a Parallel Multistage Decision-Feedback (PMDF) strategy for MA Interference (MAI) mitigation. In the user-asymptotic case, we make use of Variational Calculus (VC) techniques to derive the optimum energy allocation function that maximizes the network throughput under synchronous access when: (i) user transmissions are subject to a long-term average energy constraint; (ii) users share the same practical Forward Error Correction (FEC) code and modulation scheme, characterized by a known Packet Error Rate (PER) curve. Exhaustive simulations and comparative performance analyses are carried out using two representative FEC codes.

Resum

La interferència multiusuari constitueix el factor més limitant en el rendiment d'una xarxa, especialment quan es despleguen sistemes densos sense fils que suporten elevades càrregues de tràfic. Les polítiques de cancel·lació d'interferències (IC) són eines inestimables per a combatre aquest problema. Tanmateix, l'èxit d'aquest tipus d'esquemes IC depèn en gran mesura de la distribució de potència rebuda. En aquest treball, considerem una xarxa d'Accés Múltiple (MA) i espectre eixamplat amb un nombre massiu d'usuaris per una àmplia àrea de comunicacions Màquina a Màquina (M2M) on el node central implementa una estratègia *Parallel Multistage Decision-Feedback* (PMDF) per mitigar la interferència MA (MAI). En el cas asimptòtic d'usuaris, fem ús de tècniques de Càlcul Variacional (VC) per derivar la funció òptima d'assignació d'energia que maximitza el rendiment de la xarxa d'accés síncron quan: (i) les transmissions dels usuaris estan subjectes a una restricció d'energia promig al llarg del temps; (ii) els usuaris comparteixen el mateix codi *Forward Error Correction* (FEC) i esquema de modulació pràctics, caracteritzats per una corba *Packet Error Rate* (PER) coneguda. S'han dut a terme simulacions exhaustives i anàlisis comparatives de rendiment utilitzant dos codis FEC representatius.

Resumen

La interferencia multiusuario constituye el factor más limitante en el rendimiento de una red, especialmente cuando se despliegan sistemas densos inalámbricos que soportan elevadas cargas de tráfico. Las políticas de cancelación de interferencias (IC) son herramientas inestimables para combatir este problema. Sin embargo, el éxito de tales esquemas IC depende en gran medida de la distribución de potencia recibida. En este trabajo, consideramos una red de Acceso Múltiple (MA) y espectro ensanchado con una cantidad masiva de usuarios para una amplia área de comunicaciones Máquina a Máquina (M2M) donde el nodo central implementa una estrategia *Parallel Multistage Decision-Feedback* (PMDF) para mitigar la interferencia MA (MAI). En el caso asintótico de usuarios, hacemos uso de técnicas de Cálculo Variacional (VC) para derivar la función óptima de asignación de energía que maximiza el rendimiento de la red de acceso síncrono cuando: (i) las transmisiones de los usuarios están sujetas a una restricción de energía promedio a lo largo del tiempo; (ii) los usuarios comparten el mismo código práctico *Forward Error Correction* (FEC) y esquema de modulación, caracterizados por una curva *Packet Error Rate* (PER) conocida. Se han realizado simulaciones exhaustivas y análisis comparativos de rendimiento utilizando dos códigos FEC representativos.

A la Laura,

Acknowledgements

En primer lloc, i sense dubte, Javier Villares, m'agradaria donar-te el meu sincer agraïment per dipositar la teva confiança en mi a l'hora de proporsar-me per dur a terme aquest treball. Gràcies també per la teva motivació i en especial, per ajudar-me en tots els moments durs del treball, que han estat molts.

El meu segon agraïment és pel Josep Sala, pel teu incondicional compromís amb mi, amb el PIC perepunyetes, per les lliçons de càlcul variacional i per les teves directrius de treball. No sabria quantificar el nombre de coses que he après al teu costat, parlo de raonaments, metodologies... Josep, ets el capo! Sóc conscient que durant aquest temps, volguent o no, tu has estat un pilar fonamental de cara a decidir el meu futur professional. Espero que: tal i com està previst, poguem seguir colaborant junts en més projectes...

Més agraïments pel Francesc Rey, pel teu suport, per les teves aportacions enfocades a ajudar "a no tancar l'empresa", per les teves anècdotes i per les teves correccions.

Per últim, i no menys important, als meus pares i germanes, al grup d'amics de la ETSETB del grau i màster, que fa un temps ens vam dividir i espero que ens tornem a trobar aviat.

Finalment, a la LAURA, peça clau d'aquest treball i del nostre projecte.

Francesc Molina, Barcelona 2017

This work has been carried out under the scope of projects TEC2013-47020-C2-2-R (COMPASS) and TEC2016-76409-C2-1-R (AEI/FEDER, UE) (WINTER): Ministerio de Economía, Industria y Competitividad (Spanish administration); 2014 SGR 60: AGAUR (Catalan administration). Documentation for a refereed scientific publication is currently underway.

Contents

List of Figures

Chapter 1

Introduction

This thesis is the result of one year's work at the Signal Processing and Communications Group (SPCOM) under the framework of VC-based IC strategies for massively populated wireless networks operating in the user-asymptotic regime.

The present document provides a detailed exposition of the most important contributions achieved during this period since the original formulation of the objectives. The initial stage of the research involved an in-depth study on the foundations and tools of VC (mainly [1]), together with the support of unofficial interactive seminars on the subject taught by the directors of the thesis.

Progress towards a final and complete understanding of the solution, as is commonplace in research, has been fraught with unexpected obstacles, both on the theoretical and practical sides of the problem. It is in this respect that the author believes the most attractive way to present the corresponding developments is one which reflects, precisely, that evolution.

1.1 State of the art

The fifth generation (5G) of communication systems is expected to motivate the use of smart devices with improved network and device capabilities [2,3]. The arrival of 5G cellular systems will potentially be a key driver for the yet to emerge global Internet of Things (IoT) [4]. IoT refers to a highly interconnected heterogeneous network of entities providing new services and applications for human interests [5]. It is envisaged that new technologies with several forms of data traffic and different delay, bit-rate, reliability and energy consumption will arise in the following years [6]. In that respect, M2M communications were conceived to make the totally autonomous operations of the networked devices possible. They enable faster, safer and more reliable communications when compared with those under human supervision [7].

Today's communication systems should be able to serve large-population networks with a shared and finite amount of resources. However, nowadays, this is not feasible due to the fact that current networks are not prepared to manage the increment in the number of users as a consequence of IoT. This will lead to the need of developing very refined physical and media access control layer technologies that can better exploit the radio channel [8].

Random Access (RA) communications have gained a lot of momentum in networks where the signalling delay and/or the use of feedback channels makes the user coordination task difficult [9]. The earliest devised RA protocol is the well-known ALOHA [10], widely extended in satellite communications networks of uncoordinated devices. Several variants have been developed, such as slotted-ALOHA, obtaining significant throughput improvements with respect to the baseline ALOHA, at the cost of requiring user packet

synchronization (alignment) at reception [10]. Novel approaches have been conceived such as Diversity Slotted Aloha, in which each packet is sent twice in different slots, which improves the performance of the prior ALOHA systems under moderate load conditions [11]. In all cases, the main limiting factor to network performance is the amount of MAI.

Code-Division-Multiple-Access (CDMA) allows simultaneous user transmissions while sharing the same broadband resource, which opens up the possibility of using CDMA in RA communications scenarios. In this case, network subscribers spread their packets before transmission in order to access the channel in a quasi-orthogonal way. Moreover, CDMA transmissions are also beneficial thanks to a greater immunity to channel impairments and dynamic channel sharing [12]. As an added advantage, user asynchronism can be easily dealt with CDMA making use of multiuser receivers [13].

Multiuser detection (MUD) of simultaneous and independent CDMA user-transmissions has been widely investigated by S.Verdú [14]. It is derived therein that the optimum detector needs joint user-detection where perfect knowledge of all user-signatures and channel impulse responses is required. Maximum Likelihood Sequence Estimator (MLSE) is indeed the optimal detector. In the case of synchronous access, the K-user MLSE consists of a bank of optimum single-user detectors operating independently, whereas in the asynchronous case consists of a bank of single-user matched filters followed by a Viterbi algorithm [15]. In both cases, the computational complexity of such MUDs increases exponentially with the number of users, which is not feasible for practical implementations, especially in networks with a large number of users [16].

In low-rate communication scenarios over a dense user population, new access techniques have been devised for exploiting inter-user collisions as a means of increasing spectral efficiency [17, 18]. Different multiuser schemes implementing Direct-Sequence (DS) CDMA (DS-CDMA) together with IC policies have been studied, obtaining improvements with respect to conventional CDMA [14,19,20]. In particular, Successive IC (SIC) and multistage Decision-Feedback (DF) receivers with IC capabilities (parallel or successive) have been presented as the main architectures with successful MAI mitigation [21,22].

Anyway, the performance of such IC schemes is highly dependent on the received power distribution [23]. To enable power control, different variants have been broadly investigated. As studied in [24], there exist two alternative approaches for energy allocation: random and deterministic. In the first case, users randomly select their transmitted energy from a continuous probability distribution, while in the deterministic approach the transmitted energy is set depending on each user's current channel state.

For several years, asymptotic analyses of large-CDMA systems, where both the number of users and the spreading gain increase to infinity while keeping their ratio constant, have gained a lot of interest [12]. In these user-asymptotic cases, several analyses techniques can be applied, such as: VC [24], Random Matrix Theory [25] or the Replica Method [26], among others. In this work, we only employ VC techniques to optimize a global utility (spectral efficiency) in the user-limit case. In [27], the authors consider a many-user SIC scenario for deriving the optimal signal-to-interference-plus-noise ratio (SINR) profile in terms of spectral efficiency. In [28], Sala et al. derive the user-asymptotic symbol energy profile that maximizes the average spectral efficiency when a constraint on the power imbalance of received users is enforced. In [29], the optimum distribution of ordered energies throughout SIC stages when users are required to fulfil an average energy constraint is determined.

To the best of our knowledge, few capacity studies have been carried out in terms of multistage IC policies. In [30], it is concluded that parallel IC does not improve the channel capacity in the presence of non-fading conditions. A single stage is enough to enable free-error probability in case of equal rate and power allocation when optimal codes are used. No further analyses have been found, either with the use of practical encoders or when considering imperfect cancellation. For that reason, some references

involving SIC policies are shown. It is stated in [24], that the maximum-rate SINR profile throughout SIC stages is uniform. This contrasts with the fact that when considering practical FEC codes along with imperfect cancellation, the optimum SINR profile is a decreasing function of the user ordering [29].

One of the major obstacles to the application of SIC schemes in practical wireless systems is the processing delay [31]. In dense DS-CDMA networks, unless the receiver works with clock frequencies unboundedly high, a practical SIC implementation may be unreasonable, due to the fact that the receiver must successively decode all users at every time slot. For that reason, we consider a parallel multistage detector [14], sometimes referred to as bootstrap [32,33], in which the system's latency is controlled by the number of stages, irrespectively of the number of users. Moreover, parallel multistage DF architectures are also beneficial under the near-far effects, since simultaneous processing encourages the use of similar power levels between users. Additionally, these schemes also allow to mitigate the imperfect cancellation effect, as a consequence of signal reconstructions being improved throughout the DF stages [31].

1.2 Statement of purpose

In this thesis, we consider the uplink of a massive-user network with the receiver implementing a PMDF strategy in order to mitigate MAI. The goal of this work is focused on determining the optimal energy allocation function of the coordinated spread-spectrum MA network, when user transmissions are enforced to fulfil a long-term energy constraint while using practical FEC codes and modulation schemes with a known PER curve.

We focus on the derivation of the optimal energy distribution using VC techniques [1]. Unlike VC problems studied in the literature [27–29, 34], we explore discontinuous energy allocation functions as candidates for maximizing the average spectral efficiency over all users of the network described herein.

For several reasons, the proposed scenario is of interest in the M2M context over a massive user population. Firstly, in terms of energy consumption at both the network and the device level, it is convenient to limit energy transmissions; secondly, in terms of co-channel or out-of-band interference on other neighbouring services, it is also beneficial to reduce the average energy transmitted into the channel by the whole machine network.

1.3 Thesis outline

For the rest of the document, this thesis is organized as follows;

In **Chapter 2**, we present the considered MA scenario, the transmitter's characteristics and limitations, the receiver's IC architecture, and the power control mechanism. We also develop a signal model for the considered multiuser scenario. Furthermore, finite and asymptotic user equations for the described scenario have been derived.

In **Chapter 3**, we state the VC problem that allows to derive the optimum energy allocation function that maximizes the throughput of the network presented in Chapter 2. For that reason, firstly, we describe the space of functions from which energy profile candidates are going to be considered; then, we formulate the aforementioned VC problem and we make use of VC tools to address its resolution in the case of a generic known channel. Its determination has required to derive the stationary point equation and the related transversality conditions of the constrained VC problem. Additionally, a resolution method is proposed for the case of uniform channel gains.

In **Chapter 4**, we evaluate the theoretical results over a representative interference-dominated scenario

that follows the system model described in Chapter 3.

In **Chapter 5**, we conclude and summarize the main results of this work. Finally, we propose some topics for further research.

Chapter 2

Problem Statement

The aim of this chapter is to present the studied problem. Particularly, in Section 2.1, we describe the considered scenario. In Section 2.2, we introduce the adopted PMDF scheme and we derive some expressions that model its behaviour. The following sections are devoted to stating the signal model and to the derivation of finite (Section 2.3) and asymptotic (Section 2.4) user models for the studied scenario.

2.1 Scenario description

Let us consider a massive population of $1 \leq k \leq K$ low-rate users transmitting on the uplink of a MA channel towards a central node, equipped with strong multipacket reception capabilities. Users share the same frequency band and time resources to establish communication using a non-orthogonal spread-spectrum technique. The proposed scenario is depicted in Figure 2.1.

We consider a coordinated access scheme based on a slotted-time division indexed by n. At the beginning of every time slot, users generate new information packets that are encoded together with a Cyclic Redundancy Check (CRC) using the same FEC code. The CRC enables error detection at the FEC decoder. In this way, erroneously decoded packets are discarded, and no retransmissions are contemplated. We associate the shared encoder with a known PER curve, a scalar function of the Signal-to-Noise Ratio (SNR) under the additive Gaussian model. For convenience, we will not specify the length of the appended CRC. We assume that a sufficiently long CRC exists such that its error probability is negligible.

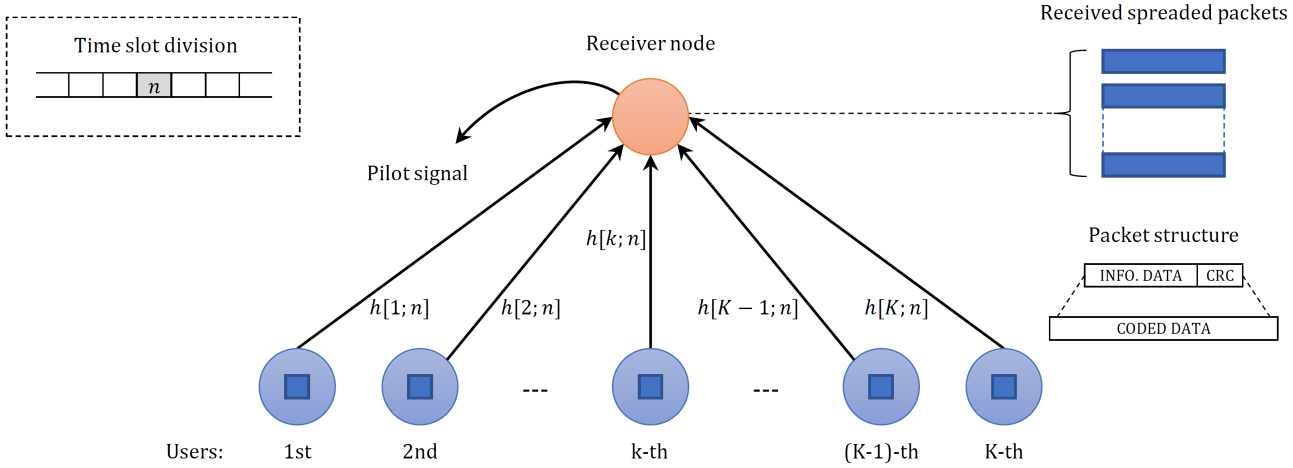

Figure 2.1: Multiple access scenario.

Energy limitation

Let $E_{\mathrm{s}}[k;n]$ be the transmitted symbol energy of the k-th user at time slot n. According to the energy efficiency concerns of machine-type communications, users are encouraged to limit their power transmissions according to a per-user average energy constraint over time of $\overline{E}$ Joules per symbol,

$$\lim_{n\to+\infty} \frac{1}{n} \sum_{i=1}^{n} E_{\mathrm{s}}[k;i] \quad = \quad \overline{E} \tag{2.1}$$

No further restriction is placed on the peak energy of the users to model the maximum amount of energy that every user's transceiver can supply. We are only concerned with the long-term average energy that users employ in their transmissions. In this situation, we allow users to access the channel using a very high peak energy as long as they average out their transmission power on the subsequent slots in order to satisfy (2.1). Of course, this corresponds to a non-practical scenario, and thus, we might force the system to work in a regime that avoids this circumstance. Nonetheless, these type of constraints are typical in the analysis of different telecommunication systems, where, in general, the solution results in a finite and moderate peak energy (e.g. [34]).

Multiple access interference and interference cancellation architecture

The amount of MAI constitutes the major contributor to the limitation of the network's performance. Several strategies may be formulated to mitigate MAI. For reasons of simplicity and without sacrificing IC capabilities, we have opted for a classical multiuser multistage detector scheme [14]. The receiver node is set to perform a PMDF strategy in which users are simultaneously decoded and cancelled from the input signal of the rest of users before proceeding to the subsequent stage. Later on, we will describe thoroughly the mentioned PMDF policy.

Channel characterization and power control mechanism

Let $h[k;n]$ be the channel power gain between the k-th user and the receiver at the n-th time slot, with known probability distribution $F_H(h) \doteq \Pr\{H \leq h\}$, independent and identically distributed over each user, slowly time-varying for $n \neq n'$ and approximately flat over the packet duration.

For simplicity, during the mathematical development, we will set the user indices in descending order of users' channel gains, as $h[1;n] \geq h[2;n] \geq \cdots \geq h[K;n]$. The reader may note that, as all users are going to be processed simultaneously (parallel multistage architecture), re-ordering is not strictly necessary. Nonetheless, re-labelling users simplifies the rest of the work as long as the mathematical treatment is simplified.

As we consider the case of identically distributed channels over the user ordering, the long-term average energy constraint (2.1) coincides with the average energy over the user population,

$$\lim_{K\to+\infty} \frac{1}{K} \sum_{k=1}^{K} E_{\mathrm{s}}[k;n] \quad = \quad \overline{E} \tag{2.2}$$

Under this infinite-user model, the distribution of the channel coefficients over all users converges to a deterministic function irrespectively of n. That is, at every time slot, users in the system will perceive the same channel realizations, but sorted differently. Therefore, and without loss of generality, we suppress the explicit time slot index n.

In order to guarantee the success of this PMDF scheme, we set a power control mechanism in which each user selects its transmitted energy $E_s[k] = a(h[k])$ according to a known energy allocation function $a(h)$ to be optimized [24]. Therefore, perfect channel knowledge needs to be available at every transmitter. Several alternatives can be followed to enable perfect channel state information at transmitters. Without entering into excessive detail, we will consider that the receiver node is regularly broadcasting a known pilot signal on a low-rate control channel, from which every user estimates $h[k]$ assuming channel reciprocity, and that the channel coherence time is sufficiently long when compared with the symbol interval.

With the focus on the proposed scenario, we seek to determine the energy allocation function $a(h)$ that maximizes the throughput of the network presented herein, when:

(i) transmitters access the channel with a deterministic energy allocation strategy subject to a long-term per-user average energy constraint of $\overline{E}$ Joules per symbol.

(ii) the receiver implements a PMDF approach in order to mitigate MAI.

The considered scenario may be exemplified if we envisage the uplink of a M2M mobile network under the DS-CDMA model. The channel gains represent the path-loss component of each user with respect to the station position, being corrupted by the instantaneous fast-fading conditions. Moreover, users may be deployed over a scarce energy-source environment and they are endowed with energy harvesting mechanisms in order to charge their batteries. Hence, users' transmissions may be power-limited so as to save energy for future access attempts according to some predefined criteria.

2.2 Parallel multistage decision-feedback scheme

The key concept behind decision-feedback detectors is the creation of separate estimates of the MAI generated by each user-contribution in order to subtract out the major part of the MAI seen by each of them. Multistage DF schemes present similarities with respect to the decision-feedback equalizers used to counteract inter-symbol interference [35]. Underlying the same principle, DF receivers have been envisaged [31].

With the attention focussed on the studied scenario, we consider that the receiver node is equipped with a bank of K single-user detectors that work in parallel along with their corresponding reconstructors, which for convenience and simplicity, are going to be referred to as D&R (Detector and Reconstructor) during the rest of the work. The central node is configured according to a multiuser parallel DF structure, which has been denoted "bootstrap" in some publications [32,33] and appears depicted below:

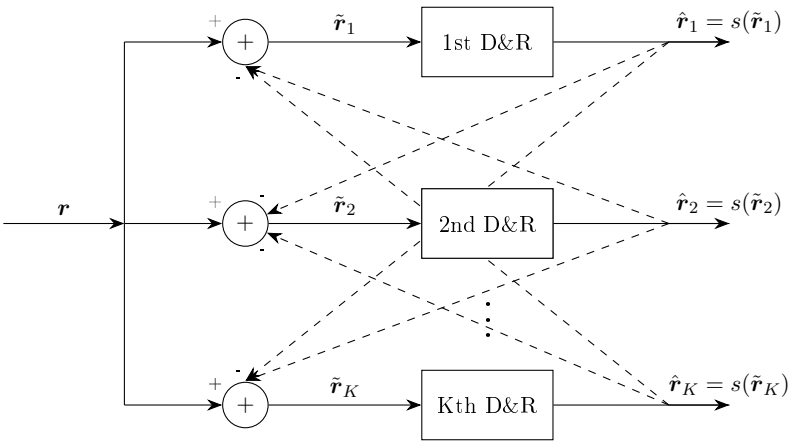

Figure 2.2: Parallel multistage decision-feedback architecture.

with $\boldsymbol{r} = [\, r[1], r[2], ..., r[N_s] \,]^T$ the received packet (of N_s samples) obtained from sampling the received waveform at a given chip rate, $\tilde{\boldsymbol{r}}_k = [\, \tilde{r}_k[1], \tilde{r}_k[2], ..., \tilde{r}_k[N_s] \,]^T$ the input signal at the k-th D&R input, $\hat{\boldsymbol{r}}_k = [\, \hat{r}_k[1], \hat{r}_k[2], ..., \hat{r}_k[N_s] \,]^T$ the k-th user's reconstructed packet and $s(\cdot)$ the function implemented by each D&R comprising the steps of de-spreading-demodulation-decoding and recoding-remodulation-spreading.

In view of the needed signals, we define the matrices $\widetilde{\boldsymbol{R}}$ and $\widehat{\boldsymbol{R}}$, which contain by columns the input and the output (reconstructed) packet signals of each D&R, respectively, as follows,

$$\widetilde{\boldsymbol{R}} \doteq \begin{bmatrix} \tilde{r}_1[1] & \tilde{r}_2[1] & \cdots & \tilde{r}_K[1] \\ \tilde{r}_1[2] & \tilde{r}_2[2] & \cdots & \tilde{r}_K[2] \\ \vdots & \vdots & \ddots & \vdots \\ \tilde{r}_1[N_s] & \tilde{r}_2[N_s] & \cdots & \tilde{r}_K[N_s] \end{bmatrix} \qquad \widehat{\boldsymbol{R}} \doteq \begin{bmatrix} \hat{r}_1[1] & \hat{r}_2[1] & \cdots & \hat{r}_K[1] \\ \hat{r}_1[2] & \hat{r}_2[2] & \cdots & \hat{r}_K[2] \\ \vdots & \vdots & \ddots & \vdots \\ \hat{r}_1[N_s] & \hat{r}_2[N_s] & \cdots & \hat{r}_K[N_s] \end{bmatrix} \tag{2.3}$$

Therefore, we have that,

$$\widehat{\boldsymbol{R}} = s(\widetilde{\boldsymbol{R}}) = s(\boldsymbol{r} \cdot \mathbf{1}^T - \widehat{\boldsymbol{R}}) \tag{2.4}$$

It is easy to see that the presented structure constitutes a discrete feedback system, since the input of each user's D&R is connected with the output of the other users' D&R. From here, we will assume that the system has at least one equilibrium point at which we are able to converge starting from the received signal $\boldsymbol{r}$. Still, no proof of the previous statement is available for the moment, nor of the conditions under which that or those points exist. This will be intuitively justified in the following lines.

This architecture reminds us of the computation of the output of an infinite impulse response filter, and so as to determine the equilibrium point (stationary regime) of the system, we unfold the previous structure into several stages of repeated architecture, as depicted in Figure 2.3. In this way, we are able to converge towards a stability point as long as it exists. It should be remarked that given the noise randomness and MAI, the uniqueness of this equilibrium point may be questioned.

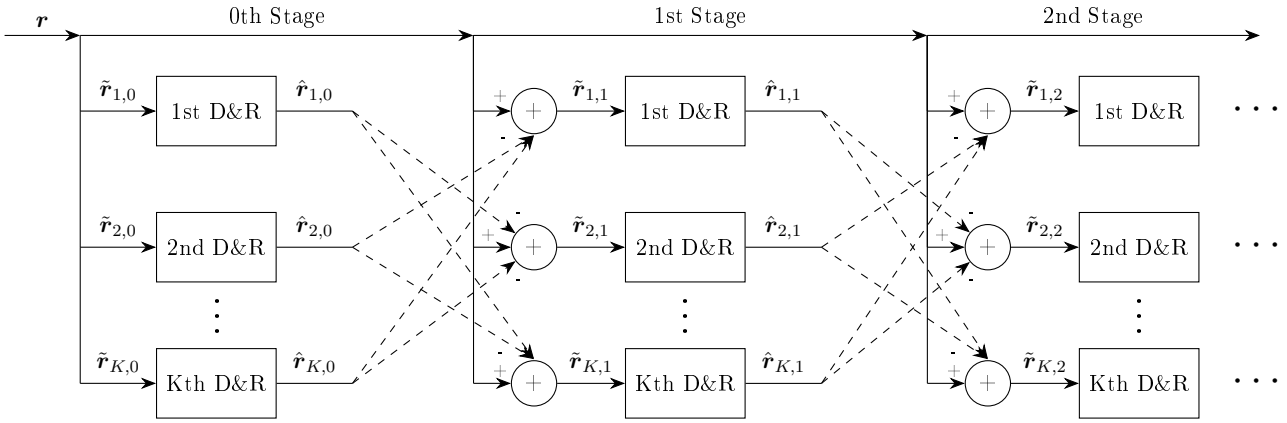

Figure 2.3: Parallel multistage decision-feedback architecture. Unfolded structure.

The unfolded structure in Figure 2.3 needs of some explanation in order to understand its behaviour. Each D&R has a target user and at any stage (i), it only operates on its own signal $\tilde{\boldsymbol{r}}_{k,i}$. We define a D&R-stage as the process whereby a D&R de-spreads its input signal $\tilde{\boldsymbol{r}}_{k,i}$, demodulates, decodes its target user, and reconstructs its user's packet if it has been correctly decoded $\hat{\boldsymbol{r}}_{k,i}$, otherwise $\hat{\boldsymbol{r}}_{k,i} = \mathbf{0}$. Then:

a) At the initial stage $(i = 0)$, all D&Rs operate on the received signal $\tilde{\boldsymbol{r}}_{k,0} = \boldsymbol{r}$.

b) At the i-th stage, those D&Rs which successfully decode their packet (CRC checking) will reconstruct

$\hat{\boldsymbol{r}}_{k,i}$ and cancel it from the received signal of the rest of D&Rs.

c) At any DF stage, every D&R operates, regardless of its success during the last stage, on $\boldsymbol{r}$ minus the contribution of all other D&Rs that satisfactorily decoded its user in the previous stage.

It is important to highlight that the intrinsic randomness of noise and MAI provokes that different users are successfully decoded in distinct stages of the decoding process. Nevertheless, and anticipating the following sections, the fraction of successfully decoded users converges to a computable quantity.

Back to the equations that describe the outspread DF architecture in Figure 2.3, we have that,

$$\widehat{\boldsymbol{R}}_{i+1} \;=\; s(\widetilde{\boldsymbol{R}}_{i+1}) \;=\; s(\boldsymbol{r}\cdot\mathbf{1}^T \;-\; \widehat{\boldsymbol{R}}_i) \tag{2.5}$$

where we have introduced the sub-index i for denoting the i-th DF stage. Note that the receiver needs enough memory to allocate the received packet $\boldsymbol{r}$ and the matrix of reconstructed packets $\widehat{\boldsymbol{R}}_i$, from which it is able to generate the rest of variables. Of course, if the system allows an stability point ($i \to +\infty$), then the previous equation matches (2.4),

$$\widehat{\boldsymbol{R}}_* \;\doteq\; \lim_{i\to+\infty} \widehat{\boldsymbol{R}}_{i+1} \;=\; s(\widetilde{\boldsymbol{R}}_*) \;=\; s(\boldsymbol{r}\cdot\mathbf{1}^T \;-\; \widehat{\boldsymbol{R}}_*) \tag{2.6}$$

with the asterisk notation to indicate the convergence point.

Comparison with related IC policies

Relating this DF architecture with well-known multiuser schemes, it must be said that the stated structure presents performance similarities when compared with those ones achieved with SIC receivers of a single iteration. It is not possible to establish beforehand a comparison between the performance of both architectures. Therefore, one must resort to direct evaluation at each scenario.

Naturally, under large population networks, the computational cost of the multistage detector increases considerably with respect to SIC schemes, although it hopefully captures the essential features of a user-asymptotic scheme while making a more simplifies mathematical treatment possible.

Mitigation of the imperfect cancellation effect

For a point of view of a practical scheme, it is widely known that perfect cancellation is unrealistic as long as the amount of MAI questions the reliability of the frequency, amplitude and phase estimations. In this case, imperfect cancellation is assumed from which an energy-fraction of each user remains after cancelling its contribution.

As opposed to SIC architectures, a DF scheme allows the mitigation of this imperfect cancellation effect. Users signals are re-estimated at each stage, and due to the fact that the interference level is reduced with each of them, this enables the users to work with higher SNRs as more stages are performed. This is beneficial seeing that the mentioned estimators enhance the accuracy of their estimates as more stages are completed.

The following sections are devoted to the derivation of finite and asymptotic user models of the DF scheme described herein.

2.3 System model and finite user characterization

We consider the DS-CDMA model in which each user generates a sequence of D symbols $\boldsymbol{s}_k$. Random and independent spreading sequences $\boldsymbol{c}_k$ are designated to the network subscribers, with processing gain N (long-code model), and assumed known at the receiver side [12]. Therefore, the transmitted complex baseband signal by the k-th user is

$$x_k(t) \;=\; A_k \cdot \sum_{i=0}^{D-1} \sum_{m=0}^{N-1} s_k[i] \cdot c_k[Ni+m] \cdot p(t-(Ni+m)T_c) \tag{2.7}$$

with A_k a complex amplitude factor, $p(t)$ the chip pulse of unitary energy and T_c the chip period.

At the receiver, as a consequence of the access synchronism, users signals are obtained with perfect packet alignment. Therefore, under the flat fading model, the complex equivalent baseband received signal after down-conversion is

$$y(t) \;=\; \sum_{k=1}^{K} \sqrt{h[k]} \cdot x_k(t) \;+\; n(t) \tag{2.8}$$

with the received signal corrupted by additive Gaussian noise $n(t)$.

At the receiver, we model MAI as additive Gaussian noise after de-spreading according to the long-code model [12]. Under this model, an average cross-correlation between different user-signatures of θ/N [36] is assumed, with θ an average decorrelation factor that models timing misalignments and carrier phase offsets.

We consider the characteristic function of the FEC decoder, PER[Γ], a known function of the SNR (Γ). Also, we assume imperfect cancellation, with $\epsilon(\Gamma[k]) \in (0,1)$ the remaining energy fraction of the k-th user after its signal cancellation (we consider a general implementation-dependent function for ϵ vs. Γ) [23]. Moreover, statistically independent decoding attempts between stages is assumed, provided that at each DF stage a significant portion of users is favourably decoded; intuitively, such an assumption is reasonable in the sense that the signal's waveform at the input of every D&R has been substantially changed after cancelling other users contributions.

Therefore, at the i-th DF stage, the SINR seen by the k-th user at the output of its de-spreader is, in agreement with the large-spreading model, given by

$$\Gamma_{i\geq 0}[k] \;=\; \frac{E_{\mathrm{r}}[k]}{N_0 + \xi_i[k]} \tag{2.9}$$

with $E_{\mathrm{r}}[k] = E_{\mathrm{s}}[k]h[k]$ the received symbol energy of the k-th user, N_0 the noise power spectral density and $\xi_i[k]$ the MAI seen by the k-th user at the i-th DF stage, defined by

$$\xi_{i\geq 1}[k] \;=\; \frac{\theta}{N} \sum_{j\neq k} \varepsilon(j|\Gamma_{i-1}[j]) E_{\mathrm{r}}[j] \tag{2.10}$$

with the initial value $\xi_0[k] = \frac{\theta}{N}\sum_{j\neq k} E_{\mathrm{r}}[j]$ and $\varepsilon(j|\Gamma)$ a binary random variable that takes values depending on the j-th decoder success: equal to 1 with probability PER[Γ] (decoding error) and equal to $\epsilon(\Gamma)$ with probability PSR[Γ] $\doteq 1 -$ PER[Γ] (successful decoding).

It is important to emphasize that the assumption of independent decoding attempts between iterations starts to take importance at this point of the work, given that, we consider independent realizations of the random variable $\varepsilon(j|\Gamma)$ at every DF stage i.

2.4 Asymptotic system characterization

This section is devoted to deriving the equations of two asymptotic analyses related with the system model showed in Section 2.3. First, in terms of users, we will consider that infinite users use sequences of large-spreading gain while keeping their ratio constant. Secondly, we also consider the receiver node implementing the described policy in Section 2.2 with an asymptotically large number of DF stages in order to evidence the equations that predict the stability point of the system.

2.4.1 User-asymptotic expressions

In the user-asymptotic case, we transform the discrete user index k into the continuous variable $t \doteq \lim_{K\to+\infty} k/K$, in which the user indices $k = 1, ..., K$ are compressed within the interval $0 < t \leq 1$ [28]. Also, we let $N \to +\infty$ so that the system's load factor $\alpha \doteq K/N$ is asymptotically fixed, given that K, N increase in the same proportion. As well, we convert:

(i) the discrete variables $\Gamma_i[k], E_{\rm r}[k], E_{\rm s}[k], h[k]$ into the continuous profiles $\Gamma_i(t), E_{\rm r}(t), E_{\rm s}(t), h(t)$, all defined within the interval $0 < t \leq 1$.

(ii) the summations into integral forms with $\mathrm{d}t \doteq \lim_{K\to+\infty} \frac{1}{K}$.

Therefore, in this user-limit regime, the energy constraint (2.2) becomes the following integral equation:

$$\int_0^1 E_s(t)\,\mathrm{d}t \;=\; \int_0^1 \frac{E_{\rm r}(t)}{h(t)}\,\mathrm{d}t \;=\; \overline{E} \tag{2.11}$$

As well, in this large-user regime, as each user constitutes an infinitesimal unit in the user continuum, all users will experiment the same MAI at every DF stage. That is, $\xi_i[k] \to \xi_i + o(1/N)$, with $o(1/N)$ an infinitesimal term and $\xi_i = \mathbb{E}\{\xi_i[k]\}$ the common user-interference level at the i-th stage. The fact that ξ_i converges to its mean value needs the assumption that function $E_{\rm r}(t)$ must be sufficiently smooth so as to consider that over every interval $[t, t+\mathrm{d}t]$ there are enough users as to ensure the mentioned convergence in probability. Therefore, (2.9 - 2.10) are turned into the following[1]

$$\Gamma_i(t) \;=\; \frac{E_{\rm r}(t)}{N_0 + \xi_i} \tag{2.12}$$

$$\xi_i \;=\; \alpha\theta \int_0^1 \left(1 - (1 - \epsilon(\Gamma_{i-1}(t)))\,\mathrm{PSR}\left[\Gamma_{i-1}(t)\right]\right) E_{\rm r}(t)\,\mathrm{d}t \tag{2.13}$$

with the initial value $\xi_0 = \alpha\theta \int_0^1 E_{\rm r}(t)\,\mathrm{d}t$, that is, at the first stage all users see the overall interference. Note that under this user-limit regime, the asymptotic continuous SINR profile $\Gamma(t)$ is proportional to the received symbol energy profile $E_{\rm r}(t)$. For mathematical convenience, and, with the intention to relate this work with previous works [29], we define $\Phi[\Gamma] \doteq \theta(1 - \epsilon(\Gamma))\Gamma \cdot \mathrm{PSR}[\Gamma]$, a known function which only depends on the decoder's system implementation. Therefore, we define

$$f(\xi_i) \;\doteq\; \alpha(N_0 + \xi_i) \int_0^1 \left(\theta\Gamma_i(t) - \Phi\left[\Gamma_i(t)\right]\right)\,\mathrm{d}t \tag{2.14}$$

from which the subsequent interference level, ξ_{i+1}, can be obtained using f, as follows: $\xi_{i+1} = f(\xi_i)$. Therefore, the interference level seen by users at each stage can be perfectly described by the succession

[1] The integrand of (2.13) is obtained by setting $E_{\rm r}(t)$ with probability $\mathrm{PER}[\Gamma_{i-1}(t)]$ (packet loss) and $\epsilon(\Gamma_{i-1}(t))E_{\rm r}(t)$ with probability $\mathrm{PSR}[\Gamma_{i-1}(t)]$ (successful decoding). Reorganizing terms, it can be proven the equivalence with (2.13).

$\{\xi_i\}_{i\geq 0} = \{\xi_0, \xi_1, \xi_2, ...\} = \{\xi_0, f(\xi_0), f(\xi_1), ...\}$. At this point, in this user-limit regime, as every user constitutes an infinitesimal unit over the user continuum, one reader can erroneously think that user contributions do not mitigate the overall interference. However, at each stage an infinite number of infinitesimal user contributions are cancelled, and thus, the initial MAI is lessened. In fact, using bounds on PSR[Γ] and $\epsilon(\Gamma)$, it is easy to see that the succession of interference levels decreases monotonically under the assumption of PSR[Γ] and $\epsilon(\Gamma)$ being increasing and decreasing functions of Γ, respectively.

2.4.2 Fixed point user-asymptotic expressions

In this section, we analyse the user-limit expressions (2.12) and (2.14) when the PMDF detector performs a large number of stages, so as to evidence the existence of a stability point along with its determination. The results take the form of a fixed point (FP) equation.

Hence, with an asymptotic number of DF stages ($i \to +\infty$), we obtain

$$\Gamma_*(t) \;=\; \frac{E_{\mathrm{r}}(t)}{N_0 + \xi_*} \tag{2.15}$$

$$\xi_* \;=\; f(\xi_*) \;=\; \alpha(N_0 + \xi_*) \int_0^1 \left(\theta\Gamma_*(t) - \Phi\left[\Gamma_*(t)\right]\right)\, \mathrm{d}t \tag{2.16}$$

where we have incorporated the asterisk sub-index for denoting the user-asymptotic SINR profile $\Gamma_*(t)$ at the final interference level $\xi_* \doteq \lim_{i\to+\infty}\{\xi\}_i$. Note that (2.16) constitutes a FP equation defined by $\xi_* = f(\xi_*)$ whose associated sequence of interference levels $\{\xi\}_{i\geq 0} = \{\xi_0, \xi_1, ..., \xi_*\}$ can be found using recursive substitution.

From here, this section continues by deriving interesting properties of the function f (2.16).

(a) *Property 1. Domain and codomain*

It is easy to see that $f : \xi \in \mathbb{R}^+ \longrightarrow (\xi_{\min}, \xi_{\max})$, that is, f is bounded by $(\xi_{\min}, \xi_{\max})$ with

$$\xi_{\max} \;\doteq\; \lim_{\xi\to+\infty} f(\xi) \;=\; \alpha\theta \int_0^1 E_{\mathrm{r}}(t)\, \mathrm{d}t \;=\; \xi_0 \tag{2.17}$$

$$\xi_{\min} \;\doteq\; \lim_{\xi\to 0} f(\xi) \;=\; \xi_0 \;-\; \alpha N_0 \int_0^1 \Phi\left[\frac{E_{\mathrm{r}}(t)}{N_0}\right]\, \mathrm{d}t \;\leq\; \xi_{\max} \tag{2.18}$$

where ξ_0 is the initial interference level value and $\xi_{\min}$ denotes the minimum value that reaches $f(\xi)$.

(b) *Property 2. Continuity and differentiability*

$f(\xi)$ is a continuous and differentiable function over all points of its domain provided that the curves PER[Γ] and $\epsilon(\Gamma)$ are chosen as continuous and differentiable too.

(c) *Property 3. Monotonicity*

We compute the derivative of $f(\xi)$ (2.16), that we denote by $f'(\xi)$, below,

$$f'(\xi) \;=\; \alpha \int_0^1 \left(\Phi'\left[\Gamma(t)\right]\Gamma(t) - \Phi\left[\Gamma(t)\right]\right)\, \mathrm{d}t \tag{2.19}$$

with $\Phi'[\Gamma] = \theta(1-\epsilon(\Gamma))(\mathrm{PSR}[\Gamma] + \Gamma\cdot\mathrm{PSR}'[\Gamma]) - \theta\epsilon'(\Gamma)\Gamma\cdot\mathrm{PSR}[\Gamma]$ the first derivative of $\Phi[\Gamma]$. It is easy to see that f increases monotonically as long as PSR[Γ], $\epsilon(\Gamma)$ are strictly increasing and decreasing functions of Γ, respectively. By definition, PSR[Γ] is increasing, and the assumption of $\epsilon(\Gamma)$ to be decreasing is realistic given that the higher the SNR, the better the receiver is able to reconstruct and cancel each user's signal.

(d) *Property 4. Limit on the interference level*

As f is increasing and bounded, the sequence of interference levels $\{\xi_i\}_{i\geq 0}$ is bounded too and decreases monotonically until it reaches a minimum given by $f(\xi_*) = \xi_*$, with ξ_* the convergence point. Therefore, f has at least one FP.

Problematics of having multiple FPs

As stated in the previous lines, f is a bounded and continuous monotonic increasing function with at least one FP, but, in general, its uniqueness cannot be guaranteed. The fact that f can have more than one FP brings along some mathematical difficulties, as will be exemplified throughout the work.

The following paragraph is dedicated to clarifying why the equation $f(\xi_*) = \xi_*$ is not sufficient for solving the posterior VC problem when multiple FPs exist. Let us consider a scenario in which the system variables along with the selected energy profile generate a function f with several FPs. Since we are only interested in determining the interference level at the best FP, it seems wise to introduce the single constraint $f(\xi_*) = \xi_*$ over the optimization problem. Indeed, the optimization problem would seek the optimum energy profile such that it generates a FP on the interference level as imposed by the said constraint. However, the enforced restriction does not suffice, since, in no case, does it ensure that the FP ξ_* can be attained from the initial interference level ξ_0 according to the discrete algorithm described. In other words, a potentially tough problem combining discrete mathematics (recursive substitution algorithm) and continuous optimization seems to arise.

The question is now, whether a way exists to map this discrete algorithm onto a simple constraint so as to be incorporated into the optimization problem.

Fixed point reachability constraint

Based on a geometrical interpretation (graphical proof) of the described recursive substitution algorithm, we present an equation that allows to know if it is possible, given a fixed point of f, to achieve it from the initial interference level ξ_0.

Proposition: Let ξ_* be a FP of f, $f(\xi_*) = \xi_*$. Therefore, a necessary and sufficient condition for ensuring the convergence of the recursive substitution algorithm to ξ_* from the initial value ξ_0 is that

$$\boxed{f(\xi) < \xi \text{ for } \xi > \xi_*} \tag{2.20}$$

It is easy to see in the example depicted in Figure 2.4 that the succession of interference levels describe a staircase function (black line) starting from the initial level ξ_0 to the convergence level ξ_*.

Proof: Using *Property 1*, we have that $\forall \xi, f(\xi) \leq \xi_0$, that is, f is always found below the initial point ξ_0. In particular, as $\xi_1 = f(\xi_0) < \xi_0$ is verified, and recalling the graphical proof in Figure 2.4, a necessary and sufficient condition for ensuring the convergence of the recursive substitution algorithm to the interference level ξ_*, starting from ξ_0, is that (2.20) was satisfied with strict inequality.

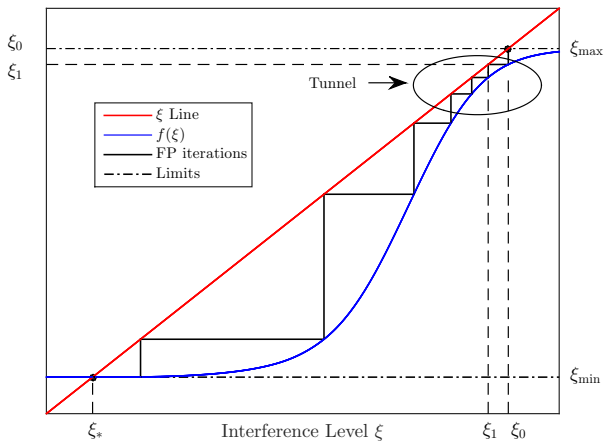

Figure 2.4: An example of the FP algorithm.

Although in the attached figure, and in the performed simulations, it is highlighted that $f(\xi) > \xi$ for $\xi < \xi_*$, it is not a necessary condition for ensuring the convergence of the algorithm to the FP ξ_*, and we are not able to guarantee its accomplishment for an arbitrary scenario parameters.

Note that depending on the evaluated parameters and the selected energy profile, the stated constraint may impose a situation in which the curve $f(\xi)$ is practically tangent to the ξ line. In this case, we will call the *tunnel* the space between both functions.

From a theoretical point of view, it does not pose any additional problem other than the fact that the receiver must perform a large number of stages in order to pass the tunnel. This matter may lead to latency issues. Let us define the δ-constriction as

$$\delta \doteq \min_{\xi} |f(\xi) - \xi|_{\xi > \xi_{\text{th}}} \tag{2.21}$$

which denotes the minimum tunnel width and ξ_{th} a threshold value in order to discard ξ-points near the FP ξ_*. The limit case would occur when $\delta \to 0$, and thus, the receiver must perform an infinite number of stages in order to pass the tunnel.

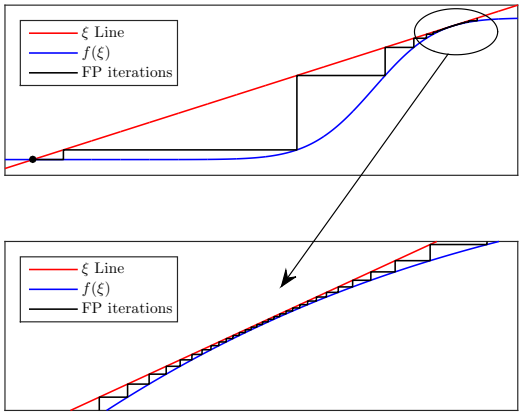

Figure 2.5: Example of a constricted tunnel.

In Figure 2.5 we depict an example of a constricted tunnel (upper part). The lower part of the attached figure is zooming into this closed aperture in order to evidence what is happening inside the tunnel. As shown, the algorithm slowly progresses inside the tunnel until it reaches the end. In particular, at each DF stage, the receiver decodes a slightly greater fraction of users such that, the amount of inter-user interference is diminished throughout DF stages by means of cancelling these users' contributions.

Moreover, there is an additional issue why it is not appropriate to have functions with constricted tunnels. Contrary to the user-asymptotic case, in the finite-user case, every user sees different MAI levels at any stage $\xi_i[k]$. This fact, may force the system to converge to an unexpected FP (crossing the ξ line). In order to avoid that, it is worth to introduce a tunable parameter in order to control the closeness of the curve f to the ξ line. Therefore, it is convenient to bound the function f from above by using an arbitrary function g in order to keep the tunnels open.

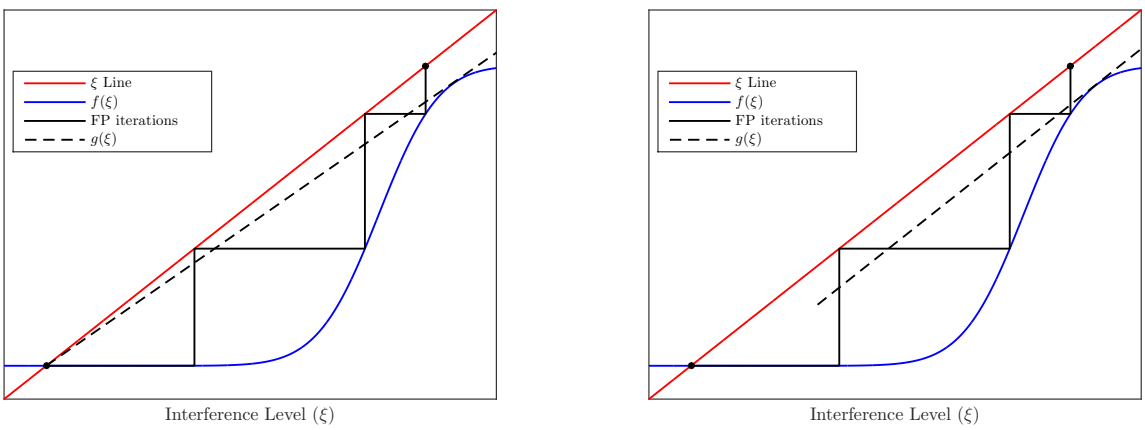

Figure 2.6: Examples of f bounded from above by two different g.

In Figure 2.6 we show for the same f curve two examples of different g bounds. In particular, we depict the cases of $g(\xi) = \Delta(\xi - \xi_*) + \xi_*$ (left) and $g(\xi) = \xi - \Delta$ (right) corresponding to the cases of variable and constant tunnel apertures, respectively. For now, the preference over what function g would be the most reasonable of choice is unknown. We have solely presented examples with the aim of giving a degree of freedom to the reader to decide and evaluate the function that best suits in his scenario.

For the attached figures, we show a limit situation in which f is practically tangent to g. Both cases will constrain the admissible energy profiles given that $f(\xi) < g(\xi)$ must be satisfied. The reader should note that by means of adjusting this function g, the receiver is able to control the latency throughout the DF stages.

Nonetheless, the evaluation of this g function is out of the scope of this work, and from here, we will consider the limit scenario in which we set $g(\xi) = \xi$. It is important to highlight that the presented constraint in (2.20) must be enforced over the optimization problem with the non-strict inequality sign. That is,

$$\boxed{f(\xi) \leq \xi \text{ for } \xi \geq \xi_*} \tag{2.22}$$

Therefore, a limit situation will be forced, in which f may reach the ξ line, i.e. $\delta = 0$. Afterwards, an intentioned imbalance over the stationary point solution will be performed in order to open the tunnels. Several strategies may be implemented in order to perform the mentioned imbalance. For reasons of simplicity, and with the intention to relate this with the previously defined δ variable, we will consider a load imbalance in which, once the optimum profile for the traffic load α is determined, we keep reducing α until the defined δ constriction is fulfilled.

Chapter 3

Problem Formulation

This section is dedicated to stating the VC problem that maximizes the overall system's spectral efficiency in the user-asymptotic case. Before that, in Section 3.1 we describe the function space from which energy profile candidates are going to be considered. In Section 3.2, we derive the stationary point equation along with the transversality conditions. In Section 3.3, we particularize the obtained expressions for the case of constant channel gains and we end up with the solution procedure to the corresponding problem.

3.1 Function space description

Calculus of Variations or *Variational Calculus* is the field of mathematics that deals with the optimization of functionals, i.e. mappings from a space of functions to the real field. Therefore, VC addresses the problem of finding the function that optimizes a global utility under predefined constraints. Before stating the VC problem of interest, we first describe the considered function space, which, in general, strongly determines the nature of the solution.

In the literature, there exist several works addressing VC problems in the framework of IC schemes [27–29, 34] where the authors derive optimal energy distributions when the user ordering is established as a function of the channel gains. In all these works, the authors considered continuously differentiable energy allocation functions $E_{\mathrm{s}}(t)$ along with a user admission index t_1, enabled when the traffic load exceeds a threshold value for which the optimum energy profile is set to zero: $E_{\mathrm{s}}(t) = 0$ for $t \geq t_1$. In our case, we consider $h(t)$ a continuous decreasing function of the user variable t. Therefore, we expect that the received energy profile $E_{\mathrm{r}}(t)$ that optimizes the presented problem will be also a decreasing function of the user ordering.

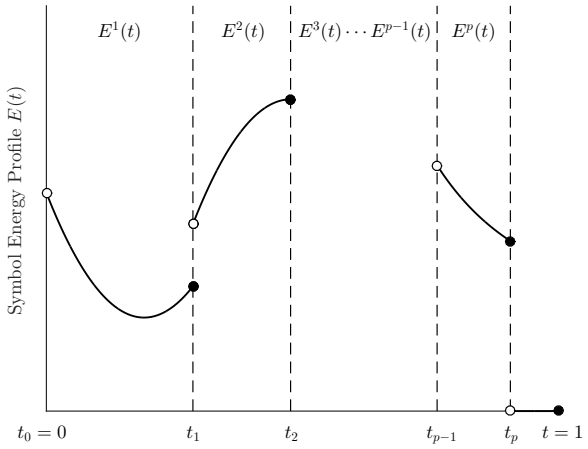

Figure 3.1: Energy profile candidates.

For the moment, although the prior statement may lack mathematical rigour, it certainly makes sense since users associated with better channel conditions are expected to achieve higher SINR at reception. Hence, we will focus the subsequent derivation on the maximization of the spectral efficiency over the received symbol energy profile, an ordered energy distribution over the user variable t.

We extend the VC problems proposed in the aforementioned works by exploring discontinuous energy allocation functions as candidates to maximize the system's throughput of the network described herein. We consider p-piecewise continuously differentiable energy profiles in the interval $0 \leq t \leq t_p$ except possibly at a finite number of points $0 < t_1, t_2, ..., t_{p-1} < t_p$. In this case, it should be noted that t_p takes the role of a user admission index. For the rest of the document, 0 and t_p will be denoted as end points while each of the points $t_1, ..., t_{p-1}$ will be referred as corner points.

Therefore, we define the normed space $\mathcal{D}$, consisting of all p-piecewise continuously differentiable functions $E(t)$ (except at some points) defined within the users partition $\tau \doteq \{t_0 = 0, t_1, ..., t_{p-1}, t_p \leq 1\}$, as depicted in Figure 3.1. The following metric is used in [1] in case of continuous functions with discontinuous derivative,

$$||E(t)|| \doteq \sum_{k=1}^{p} \left(\max_{t_{k-1} \leq t < t_k} |E(t)| + \max_{t_{k-1} < t < t_k} |\nabla_t E(t)| \right) \tag{3.1}$$

In our case, in order to allow discontinuous functions we may relax the previous norm up to

$$||E(t)|| \doteq \int_0^{t_p} |E(t)| \, \mathrm{d}t \tag{3.2}$$

Anyway, the scope of this work is not to evaluate the suitability of either of these metrics. However, the reader needs to be familiarized with the metric under which we will assume differentiability.

Last but not least, it is important to highlight that, in VC problems, there is no such *universal* space, and thus, it is not possible to find the best solution of a given problem, as it may depend on the assumed space. In this work, we have tested that discontinuous functions provide better performance when compared with that achieved using continuous ones. Under any circumstances, we consider that $\mathcal{D}$ is, to all intents and purposes, a sufficiently general space.

3.2 Optimization problem: the known channel case

In the user-asymptotic case, we address the optimization of the overall system's spectral efficiency SE [bps/Hz] $\doteq \alpha \overline{\mathrm{psr}}_* R_\mathrm{c} \log_2(N_\mathrm{sym})/(1+\beta)$, with R_c the FEC code rate, N_sym the number of symbols in the constellation, β the roll-off factor of the shaping pulse and $\overline{\mathrm{psr}}_*$ the average PSR over all users at the FP ξ_*, defined below,

$$\overline{\mathrm{psr}}_* \doteq \int_0^{t_p} \mathrm{PSR}\left[\frac{E_\mathrm{r}(t)}{N_0 + \xi_*}\right] \mathrm{d}t = \sum_{k=1}^{p} \int_{t_{k-1}}^{t_k} \mathrm{PSR}\left[\frac{E_\mathrm{r}(t)}{N_0 + \xi_*}\right] \mathrm{d}t \tag{3.3}$$

In $\mathcal{D}$, we define the constrained VC problem for maximizing the functional $\overline{\mathrm{psr}}_*$ (3.3) within the users partition τ over the received energy profile $E_\mathrm{r}(t)$,

$$\max_{\tau,\, E_\mathrm{r}(t)} \left[\overline{\mathrm{psr}}_* = \sum_{k=1}^{p} \int_{t_{k-1}}^{t_k} \mathrm{PSR}\left[\frac{E_\mathrm{r}(t)}{N_0 + \xi_*}\right] \mathrm{d}t \right] \tag{3.4}$$

$$\text{s.t.} \quad \overline{E} = \sum_{k=1}^{p} \int_{t_{k-1}}^{t_k} \frac{E_\mathrm{r}(t)}{h(t)} \, \mathrm{d}t \tag{3.5}$$

$$\text{s.t.} \quad \xi_* = f(\xi_*) = \alpha(N_0 + \xi_*) \sum_{k=1}^{p} \int_{t_{k-1}}^{t_k} \left(\theta \Gamma_*(t) - \Phi[\Gamma_*(t)]\right) \, \mathrm{d}t \tag{3.6}$$

$$\text{s.t.} \quad 0 \geq f(\xi) - \xi \quad \forall\, \xi > \xi_* \tag{3.7}$$

We subject the VC problem to: (i) the transmitter's energy constraint (3.5); (ii) the FP equation (3.6) along with the set of constraints (3.7) that guarantee the achievability of the FP, ξ_*, after performing an intentional imbalance over the stationary point solution (see the end of Section 2.4).

It is important to highlight that, as in [27–29, 34], we implicitly assume that the optimum distribution of ordered energies that fulfils the constrained VC problem is non-negative. That is, we do not impose additional constraints over the stated problem in order to enforce the non-negativeness of $E_{\mathrm{r}}(t)$, understanding that the admission user index t_p will be enabled before $E_{\mathrm{r}}(t)$ becomes negative. Anyhow, the reader may feel free to replicate the stated VC problem by incorporating a function of slack variables in order to impose the non-negativeness of the solution profile. In this case, since we address the deterministic channel case, it does not make sense to allocate zero energy to a user while assigning energy to a user with worse channel conditions. Hence, this set of slack variables reduces to a single scalar denoting the first user with zero-energy allocation, which seems closely related with the introduced user admission index t_p.

It should be mentioned that, in fact, the set of inequalities (3.7) only apply in the range $\xi_* < \xi \leq \xi_0$. Nonetheless, as $\forall \xi \ f(\xi) \leq \xi_0$ (see Section 2.4.2), we decided to extend the margin up to $\xi_* < \xi < +\infty$. It can be proven that this abuse may imply consequences during the determination of the optimal energy profile of the stated VC problem if we bound f from above with an ad-hoc function $g(\xi) < \xi$ in order to leave the tunnels open. Otherwise, the equivalence between both cases is guaranteed.

Let $u \doteq \frac{\xi_*}{N_0+\xi_*}$ denote the normalized MAI with respect to the overall noise plus MAI at the FP ξ_*, obtained dividing (3.6) by $N_0 + \xi_*$,

$$u \ = \ \alpha \sum_{k=1}^{p} \int_{t_{k-1}}^{t_k} \left(\theta \Gamma_*(t) - \Phi\left[\Gamma_*(t)\right]\right) \, \mathrm{d}t \tag{3.8}$$

which only depends on the SINR profile at this FP: $\Gamma_*(t) \doteq E_{\mathrm{r}}(t)/(N_0 + \xi_*)$. Therefore, (3.5) is re-expressed as a function of the pair $\{u, \Gamma_*(t)\}$, as follows,

$$\overline{\gamma} \ = \ \frac{1}{1-u} \cdot \sum_{k=1}^{p} \int_{t_{k-1}}^{t_k} \frac{\Gamma_*(t)}{h(t)} \, \mathrm{d}t \tag{3.9}$$

with $\overline{\gamma} \doteq \overline{E}/N_0$ the average transmitted symbol energy to noise power spectral density ratio (EsNo). Furthermore, we substitute (3.8) in (3.9) to rewrite the constraints (3.5 - 3.6) into the single restriction defined below,

$$\overline{\gamma} \ = \ \sum_{k=1}^{p} \int_{t_{k-1}}^{t_k} \left(\Gamma_*(t) \left(h^{-1}(t) \ + \ \alpha\theta\overline{\gamma}\right) \ - \ \alpha\overline{\gamma}\Phi\left[\Gamma_*(t)\right]\right) \, \mathrm{d}t \tag{3.10}$$

which only depends on the SINR profile $\Gamma_*(t)$. Moreover, introducing the definition $x \doteq \frac{N_0+\xi_*}{N_0+\xi} \in (0, 1)$, it can be proven that the set of inequality constraints in (3.7) can be defined using the previous equation when the SINR profile is substituted by $x \cdot \Gamma_*(t)$ and the equality sign is changed by the inequality sign $\geq$, as follows,

$$\overline{\gamma} \ \geq \ \sum_{k=1}^{p} \int_{t_{k-1}}^{t_k} \left(x \cdot \Gamma_*(t) \left(h^{-1}(t) \ + \ \alpha\theta\overline{\gamma}\right) \ - \ \alpha\overline{\gamma}\Phi\left[x \cdot \Gamma_*(t)\right]\right) \, \mathrm{d}t \tag{3.11}$$

Before entering into derivation details, we first define the auxiliary function

$$R \ \equiv \ R(t, \Gamma(t)) \ \doteq \ \Gamma(t) \left(h^{-1}(t) \ + \ \alpha\theta\overline{\gamma}\right) \ - \ \alpha\overline{\gamma}\Phi\left[\Gamma(t)\right] \tag{3.12}$$

Therefore, pursuing the determination of the optimal SINR profile $\Gamma_*(t)$, we rewrite the stated VC problem (3.4 - 3.7) in terms of the previously defined function, as follows,

$$\max_{\tau,\,\Gamma_*(t)} \quad \sum_{k=1}^{p} \int_{t_{k-1}}^{t_k} \mathrm{PSR}[\Gamma_*(t)]\,\mathrm{d}t \tag{3.13}$$

$$\text{s.t.} \quad \overline{\gamma} \;=\; \sum_{k=1}^{p} \int_{t_{k-1}}^{t_k} R(t,\Gamma_*(t))\,\mathrm{d}t \tag{3.14}$$

$$\text{s.t.} \quad 0 \;\geq\; \left(\sum_{k=1}^{p} \int_{t_{k-1}}^{t_k} R(t, x\cdot\Gamma_*(t))\,\mathrm{d}t \;-\; \overline{\gamma} \right) \qquad 0<x<1 \tag{3.15}$$

At this point, the reader may wonder if both VC problems, in terms of $E_{\mathrm{r}}(t)$ in (3.4 - 3.7) and $\Gamma_*(t)$ in (3.13 - 3.15), are equivalent. The answer is affirmative, and Annex B is dedicated to address its proof, together with stating the necessary procedure to determine the transmitted energy profile $E_{\mathrm{s}}(t)$ once the optimal SINR profile $\Gamma_*(t)$ has been found.

Henceforth, the subsequent sections are dedicated to solving the stated VC problem, by deriving:

(i) the Stationary Point Equation (SPE).

(ii) the corresponding Transversality Condition (TC) at every point where the extremal has a corner or a free end point.

3.2.1 Solution to the constrained VC problem: SPE and TC

We define the Lagrangian J in (3.16) that includes the functional $\overline{\mathrm{psr}}_*$ (3.13) and incorporates (3.14 - 3.15) using the function $\lambda(x)$, with $\lambda(x)_{x=1}$ used to set the equality constraint (3.14) and $\lambda(x)_{x\neq 1}$ a function of slack variables in order to impose the inequality constraints (3.15), as follows,

$$J[\Gamma_*(t)] \;\doteq\; \sum_{k=1}^{p} \int_{t_{k-1}}^{t_k} \mathrm{PSR}(\Gamma_*(t))\,\mathrm{d}t \;-\; \int_0^1 \lambda(x) \left(\sum_{k=1}^{p} \int_{t_{k-1}}^{t_k} R(t, x\cdot\Gamma_*(t))\,\mathrm{d}t \;-\; \overline{\gamma} \right) \mathrm{d}x \tag{3.16}$$

We bear in mind that $\lambda(x)_{x\neq 1} \geq 0$ is introduced according to the Karush-Kuhn-Tucker (KKT) conditions, and thus, its values are only active if it is strictly necessary, imposing the constraint with equality. Hence, by construction, we expect that only few positions of $\lambda(x)$ would be active, with $\lambda(x)_{x=1}$ always active. Advancing the solution, these positions would correspond to the FPs $\{\xi_*, \xi_*^1, ..., \xi_*^M\}$ at which f reaches the ξ line. Anyway, we will proceed with the function $\lambda(x)$, to evidence later on under which conditions it may be discretized.

Moreover, we will assume that the regularity conditions (constraint qualification) for first-order local optimality are fulfilled. In particular, we refer to the linear independence of the gradients of the constraints at the solution. Applied to VC problems, this is usually denoted the *normality* condition, and it is equivalent to requiring the matrix of constraint gradients at the solution to be of full rank [37].

From this point onwards, the rest of the section is completely dedicated to deriving the SPE and the TCs that thoroughly describe the solution procedure to this VC problem. First, let us use the auxiliary function below to group the terms inside the Lagrangian's integral (3.16),

$$F(t,\Gamma_*(t)) \;\doteq\; \mathrm{PSR}(\Gamma_*(t)) \;-\; \int_0^1 \lambda(x) R(t, x\cdot\Gamma_*(t))\,\mathrm{d}x \tag{3.17}$$

Thereafter, we assume differentiability of (3.16) with respect to $\Gamma_*(t)$, according to the chosen norm. We consider variations $v(t)$ over the SINR profile as $\Gamma_*(t) + v(t)$ and independent scalar variations δt_k over each free corner and end point $t_k \in \tau$ for $k = 1, ..., p$ as $t_k + \delta t_k$, except at $t_0 = 0$ where $\delta t_0 = 0$.

In a general case, where $F \equiv F(t, \Gamma_*(t), \Gamma'_*(t))$ and free end/corner points are admitted, it is worth taking into consideration variations $\delta\Gamma_*(t_k)$ over each t_k, as shown in [1]. In our case, as F does not depend on $\Gamma'_*(t)$, it can be proven that the effect of adding these variations would have no impact over the subsequent equations, except in one point at which this exception is clarified.

We define the increment of the functional J, as $\Delta J \doteq J[\Gamma_*(t) + v(t)] - J[\Gamma_*(t)]$, with

$$\Delta J = \sum_{k=1}^{p} \left[\int_{t_{k-1}+\delta t_{k-1}}^{t_k+\delta t_k} F(t, \Gamma_*(t) + v(t))\, \mathrm{d}t - \int_{t_{k-1}}^{t_k} F(t, \Gamma_*(t))\, \mathrm{d}t \right] \tag{3.18}$$

For convenience, we expand the integral from $[t_{k-1} + \delta t_{k-1}, t_k + \delta t_k]$ into the three following subintervals: $[t_{k-1}, t_k] \cup [t_k, t_k + \delta t_k] \cap [t_{k-1}, t_{k-1} + \delta t_{k-1}]$. Therefore, we have that,

$$\Delta J = \sum_{k=1}^{p} \left[\int_{t_{k-1}}^{t_k} \Delta F\, \mathrm{d}t + \int_{t_k}^{t_k+\delta t_k} F(t, \Gamma_*(t) + v(t))\, \mathrm{d}t - \int_{t_{k-1}}^{t_{k-1}+\delta t_{k-1}} F(t, \Gamma_*(t) + v(t))\, \mathrm{d}t \right] \tag{3.19}$$

with $\Delta F \doteq F(t, \Gamma_*(t) + v(t)) - F(t, \Gamma_*(t))$ introduced with a little abuse of notation to symbolize the increment associated with the function F. Hence, for infinitesimal first-order variations $v(t)$ and δt_k, we set $\Delta J \to \delta J$ and we expand it up to the first order, as follows,

$$\delta J\Big|_{\text{1st}} = \sum_{k=1}^{p} \left[\int_{t_{k-1}}^{t_k} \left(\frac{\partial F}{\partial \Gamma} \right) v(t)\, \mathrm{d}t + F(t_k^-, \Gamma_*(t_k^-))\delta t_k - F(t_{k-1}^+, \Gamma_*(t_{k-1}^+))\delta t_{k-1} \right] \tag{3.20}$$

Moreover, we have introduced the notation t_k^-, t_k^+ to indicate the left and right limits of every t_k. As well, $\partial(\cdot)/\partial\Gamma$ denotes the partial derivative operator with respect to Γ, with

$$\frac{\partial F}{\partial \Gamma} = \mathrm{PSR}'\left[\Gamma_*(t)\right] - \int_0^1 \lambda(x) \left(\frac{\partial R}{\partial \Gamma} \right) \mathrm{d}x \tag{3.21}$$

$$\frac{\partial R}{\partial \Gamma} = x \cdot \left(h^{-1}(t) + \alpha\theta\overline{\gamma} - \alpha\overline{\gamma}\Phi'\left[x \cdot \Gamma_*(t)\right] \right) \tag{3.22}$$

where $\mathrm{PSR}'[\Gamma]$ denotes the first derivative of $\mathrm{PSR}[\Gamma]$.

Furthermore, a key concept necessary to understand VC problems is what is called *admissible variations* (or *admissible curves*), which identifies those functions that satisfy the constraints of a given VC problem.

In our case, we define the set of admissible variations over the SINR profile, $\mathcal{V}$, comprising the set of functions (or curves) that verify the constraints (3.14 - 3.15), and the set of admissible variations over the user indices, $\mathcal{T}$, constrained by the user-index limits $[0, 1]$ as follows,

$$\mathcal{V} \doteq \left\{ v(t) \;:\; 0 < x \leq 1\,,\; \sum_{k=1}^{p} \int_{t_{k-1}}^{t_k} \left(\frac{\partial R}{\partial \Gamma} \right) v(t)\, \mathrm{d}t \leq 0 \right\} \tag{3.23}$$

$$\mathcal{T} \doteq \left\{ \delta t_k \;:\; 0 \leq t_k + \delta t_k \leq t_{k+1} + \delta t_{k+1} \leq 1 \right\} \tag{3.24}$$

where the set of inequalities in $\mathcal{V}$ only hold at those x-points where the function $\lambda(x)$ is also active.

Furthermore, we have that, for a differentiable functional, a necessary condition that an *extremal* (optimum function) must satisfy is to have $\delta J\big|_{1\text{st}} = 0$,

$$\sum_{k=1}^{p}\left[\int_{t_{k-1}}^{t_k}\left(\frac{\partial F}{\partial \Gamma}\right)v(t)\,\mathrm{d}t \;+\; F(t_k^-,\Gamma_*(t_k^-))\delta t_k \;-\; F(t_{k-1}^+,\Gamma_*(t_{k-1}^+))\delta t_{k-1}\right] \;=\; 0 \tag{3.25}$$

$$\sum_{k=1}^{p}\int_{t_{k-1}}^{t_k}\left(\frac{\partial F}{\partial \Gamma}\right)v(t)\,\mathrm{d}t \;+\; \sum_{k=1}^{p-1}\left[F(t_k^-,\Gamma_*(t_k^-)) - F(t_k^+,\Gamma_*(t_k^+))\right]\delta t_k \;+\; F(t_p^-,\Gamma_*(t_p^-))\delta t_p^- \;=\; 0 \tag{3.26}$$

which must be verified for any variation $v(t) \in \mathcal{V}$ and $\delta t_k \in \mathcal{T}$. Therefore, this reduces to considering the nullity of every term in (3.26), separately. For that reason, the ensuing sections are focussed on the analysis of each of the mentioned terms.

Stationary point equation

For the first terms in (3.26), we have that the following must vanish for any admissible variation $v(t) \in \mathcal{V}$,

$$\sum_{k=1}^{p}\int_{t_{k-1}}^{t_k}\left(\frac{\partial F}{\partial \Gamma}\right)v(t)\,\mathrm{d}t \;=\; 0 \tag{3.27}$$

At this point, the reader should be familiarized with the Fundamental Lemma of the Calculus of Variations (FLCV), which states that any extremal will satisfy $\frac{\partial F}{\partial \Gamma} = 0$ for $t_{k-1} < t \leq t_k$ when null variations at each end/corner point $v(t_k) = 0$ are considered. In our case, it is straightforward to see from [1] that in case of having no dependence in $\Gamma'_*(t)$, the previous statement is also fulfilled even if $v(t_k) \neq 0$.

Therefore, using (3.22), we obtain the following set of $k = 1, ..., p$ SPEs,

$$\boxed{\mathrm{PSR}'\left[\Gamma_*(t)\right] \;=\; \int_0^1 x\cdot\lambda(x)\cdot\left(h^{-1}(t) \;+\; \alpha\theta\overline{\gamma} \;-\; \alpha\overline{\gamma}\Phi'\left[x\cdot\Gamma_*(t)\right]\right)\mathrm{d}x \qquad t_{k-1} < t \leq t_k} \tag{3.28}$$

Transversality conditions

Moreover, from the second terms in (3.26), we get the transversality conditions at every corner $t = t_k$ given by the set of subsequent $k = 1, ..., p-1$ equations,

$$F(t_k^-,\Gamma_*(t_k^-)) \;=\; F(t_k^+,\Gamma_*(t_k^+)) \tag{3.29}$$

that is, the left and right δt_k variations must match at the corner points, which constitutes one of the Weierstrass-Erdmann (WE) conditions held at every t_k where the extremal has a corner. Substituting (3.17) into (3.29), we obtain the following $k = 1, ..., p-1$ equations,

$$\boxed{\mathrm{PSR}\left[\Gamma_*(t_k^-)\right] - \int_0^1 \lambda(x)R(t_k^-, x\cdot\Gamma_*(t_k^-))\,\mathrm{d}x \;=\; \mathrm{PSR}\left[\Gamma_*(t_k^+)\right] - \int_0^1 \lambda(x)R(t_k^+, x\cdot\Gamma_*(t_k^+))\,\mathrm{d}x} \tag{3.30}$$

In addition, for free variations over the admission user index $t_p < 1$, we have that $\Gamma_*(t_p^+) = 0$. Hence,

$$F(t_p^-,\Gamma_*(t_p^-)) \;=\; 0 \tag{3.31}$$

$$\boxed{\mathrm{PSR}\left[\Gamma_*(t_p^-)\right] \;-\; \int_0^1 \lambda(x)R(t_p^-, x\cdot\Gamma_*(t_p^-))\,\mathrm{d}x \;=\; 0} \tag{3.32}$$

We should understand that considering a space of functions allowing discontinuous solutions is not enough to guarantee that the solution will be strictly discontinuous. In fact, to guarantee that a discontinuous solution is permissible, the said extremal must fulfil the WE transversality conditions at every point where it has a corner.

3.2.2 Concerns about the inequality constraints

At this point of the work, any reader may be eager to know how many of the imposed inequality constraints should be active in order to satisfy the stated VC problem. This section is devoted to achieving this goal. The hypothesis that we have defended from the beginning of Section 3.2.1 is that the solution profile does not correspond to a continuous subset of active inequalities. Therefore, activating finite number of positions of $\lambda(x)$ is enough to fulfil the stated problem. Thus far, it was only a conjecture, which is addressed in the following lines.

Let us assume the contrary, that there exists a continuous set of slack variables activated so that a SINR profile can be found that fulfils the constrained VC problem. In terms of the interference function f, this means that there exists a continuous region $\xi_1 \leq \xi \leq \xi_2$ such that f is exactly found over the ξ line, and that by construction, $f(\xi) = \xi$ and $f'(\xi) = 1$, as depicted in Figure 3.2.

Alternatively, the same rationale can be followed using the function R and the inequalities in (3.15).

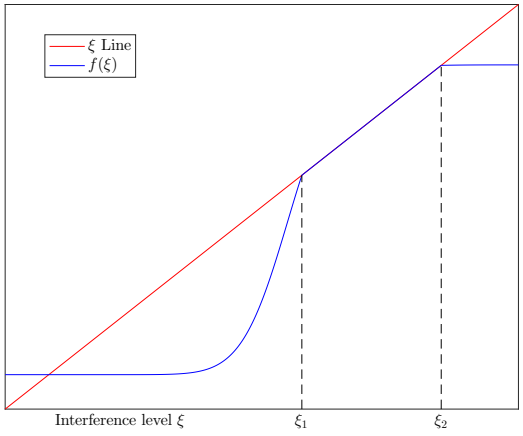

Figure 3.2: An example of an impossible f.

It is easy to see that, by construction, if the previous rationale holds, f would be non-differentiable at ξ_1, ξ_2, fact that contradicts the definition of f (see Section 2.4).

Given the results, we are able to state that at the stationary point, $\lambda(x)$ takes the form

$$\lambda(x) = \sum_{i=0}^{M} \lambda_i \delta(x - x_i) \tag{3.33}$$

with λ_i the i-th coefficient associated with the active position x_i ($x_0 = 1$), $\delta(x)$ the Dirac's delta function and M the number of active inequalities. Non activated inequalities have null associated multipliers. For convenience, during the rest of the document we are going to refer

$$\boldsymbol{\Lambda} \doteq [\, \lambda_0, \lambda_1, \dots, \lambda_M \,]^T \tag{3.34}$$

$$\boldsymbol{x} \doteq [\, 1 \ , x_1, \dots, x_M \,]^T \tag{3.35}$$

It is important to point out that, although at the stationary point $\lambda(x)$ can be discretized, any solution with an arbitrary discretization of such $\lambda(x)$ must guarantee that the initial constraint set by $\lambda(x)$ is met.

3.2.3 Constraints over the VC problem

This section is dedicated to explicitly show the constraints over the formalized VC problem as a consequence of the discretization shown in Section 3.2.2.

At the FP ξ_*, that is, for $x = 1$, as imposed from the beginning, we have that (3.14) is verified,

$$\sum_{k=1}^{p} \int_{t_{k-1}}^{t_k} R(t, \Gamma_*(t))\, \mathrm{d}t \;=\; \sum_{k=1}^{p} \int_{t_{k-1}}^{t_k} \left(\Gamma_*(t)(h^{-1}(t) \;+\; \alpha\theta\overline{\gamma}) \;-\; \alpha\overline{\gamma}\Phi\left[\Gamma_*(t)\right]\right) \mathrm{d}t \;=\; \overline{\gamma} \tag{3.36}$$

Another relevant aspect is what are the equations that those active inequalities must fulfil. For a better understanding of the following rationales, we depict in Figure 3.3 an example of the relation between both f and R functions,

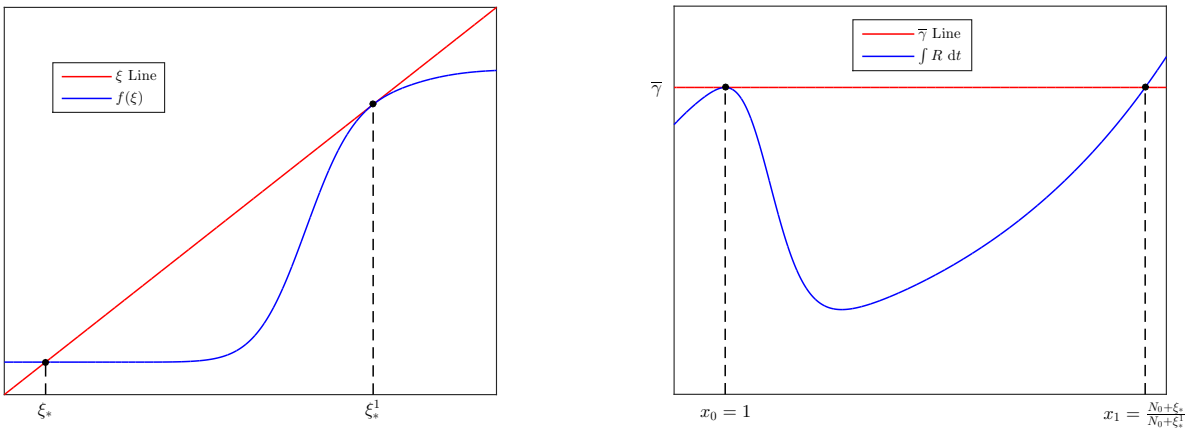

Figure 3.3: An example of the relation between f and R.

At those active inequalities $\{x_1, ..., x_M\}$, (3.15) is hold with equality. Hence, for $i = 1, ..., M$,

$$\sum_{k=1}^{p} \int_{t_{k-1}}^{t_k} R(t, x_i \cdot \Gamma_*(t))\, \mathrm{d}t \;=\; \sum_{k=1}^{p} \int_{t_{k-1}}^{t_k} \left(x_i \cdot \Gamma_*(t) \cdot (h^{-1}(t) + \alpha\theta\overline{\gamma}) - \alpha\overline{\gamma}\Phi\left[x_i \cdot \Gamma_*(t)\right]\right) \mathrm{d}t \;=\; \overline{\gamma} \tag{3.37}$$

Furthermore, by construction, as $\int R\, \mathrm{d}t \;\leq\; \overline{\gamma}$ is verified along the variable x (see the right part of Figure 3.3), this implies to acknowledge that those points where the inequality is hold with equality must be tangent to the $\overline{\gamma}$ line. Mathematically, we take the derivative with respect to the variable x at both sides of (3.37) obtaining

$$\sum_{k=1}^{p} \int_{t_{k-1}}^{t_k} \left.\frac{\partial R}{\partial \Gamma}\right|_{x_i\Gamma_*(t)} \Gamma_*(t)\, \mathrm{d}t \;=\; \sum_{k=1}^{p} \int_{t_{k-1}}^{t_k} \left(h^{-1}(t) + \alpha\theta\overline{\gamma} - \alpha\overline{\gamma}\Phi'\left[x_i \cdot \Gamma_*(t)\right]\right) \Gamma_*(t)\, \mathrm{d}t \;=\; 0 \tag{3.38}$$

It is important to highlight that we are dealing with the determination of a extremal function in a space of infinite dimensions. For that reason, in terms of computational-complexity, the determination of the optimum profile that verifies the stated equations would not be easy to address and its resolution would become, in all likelihood, a hard-computational problem. In the following section, we address a simple case in which the solution procedure of the stated VC problem is easier.

3.3 Optimization problem: the constant channel case

Given the computational complexity presented by the stated equations in the generic case of a known channel, we consider a simplification where we assume users subject to uniform channel gains $h(t) = \overline{h}$. Without loss of generality, we will incorporate these channel gains into the average EsNo by setting $\overline{\gamma} = \overline{E} \cdot \overline{h}/N_0$.

In this case, there is an ambiguity in the establishment of the user ordering as a function of the channel gains, given that all users perceive equal channel coefficients. This can be related with the fact that, when considering uniform channel gains, the deterministic energy allocation strategy coincides with a random energy selection from a continuous probability function. Therefore, with the focus on the described scenario, as we consider the deterministic energy allocation case, the feedback channel is required to assign each user its order over the variable t.

3.3.1 SPE, TCs and constraints over the VC problem

Similarly to Sections 3.2.1 and 3.2.3, in this Section we present the SPE, TCs and the constraints over the VC problem particularized for the case of uniform channel gains.

The $k = 1, ..., p$ SPEs (3.28) are turned into the following

$$\boxed{\mathrm{PSR}'\left[\Gamma_*(t)\right] \;=\; \int_0^1 x \cdot \lambda(x) \cdot \left(1 \;+\; \alpha\theta\overline{\gamma} \;-\; \alpha\overline{\gamma}\Phi'\left[x \cdot \Gamma_*(t)\right]\right) \mathrm{d}x \qquad t_{k-1} < t \leq t_k} \tag{3.39}$$

Moreover, the WE transversality conditions (3.30) at every corner t_k for $k = 1, .., p-1$ result in

$$\boxed{\mathrm{PSR}\left[\Gamma_*(t_k^-)\right] \;-\; \int_0^1 \lambda(x) R(x \cdot \Gamma_*(t_k^-))\, \mathrm{d}x \;=\; \mathrm{PSR}\left[\Gamma_*(t_k^+)\right] \;-\; \int_0^1 \lambda(x) R(x \cdot \Gamma_*(t_k^+))\, \mathrm{d}x} \tag{3.40}$$

and the additional equation (3.32) only valid when the user admission index $t_p < 1$ is turned into

$$\boxed{\mathrm{PSR}\left[\Gamma_*(t_p^-)\right] \;-\; \int_0^1 \lambda(x) R(x \cdot \Gamma_*(t_p^-))\, \mathrm{d}x \;=\; 0} \tag{3.41}$$

In this case study, (3.39) does only depend on $\Gamma_*(t)$ and not on t, and thus, the optimum SINR profile, $\Gamma_*(t)$, should be constant within each interval, yielding a multi-uniform function. Therefore, the solution would be the function with levels $\boldsymbol{\Gamma}_*$ according to the user intervals $\boldsymbol{\Delta t}$, as defined below,

$$\boldsymbol{\Gamma}_* \;\doteq\; [\,\Gamma_*^1\,,\; \ldots\,,\; \Gamma_*^p,\quad 0\quad]^T \tag{3.42}$$

$$\boldsymbol{\Delta t} \;\doteq\; [\,\Delta t_1,\; \ldots\,, \Delta t_p,\;\; \Delta t_{p+1}\,]^T \tag{3.43}$$

with $\Delta t_k \doteq t_k - t_{k-1}$ the length of the k-th user interval and $\Delta t_{p+1} \doteq 1 - t_p$ introduced to define the fraction of users assigned with zero energy.

Furthermore, with these definitions, the constraints over the VC problem (3.36 - 3.38) are analysed in the following lines. In particular, as the solution is uniform in each interval, we are able to change the integrals of every constraint for summations:

(i) For $x = 1$, (3.36) is turned into the following,

$$\boxed{\boldsymbol{\Delta t}^T R(\boldsymbol{\Gamma}_*) \;=\; \boldsymbol{\Delta t}^T \left(\boldsymbol{\Gamma}_*(1 \;+\; \alpha\theta\overline{\gamma}) \;-\; \alpha\overline{\gamma}\Phi\left[\boldsymbol{\Gamma}_*\right]\right) \;=\; \overline{\gamma}} \tag{3.44}$$

(ii) The inequality constraints at those active positions $\{x_1, ..., x_M\}$ (3.37 - 3.38) are converted into,

$$\boxed{\boldsymbol{\Delta t}^T R(x_i \cdot \boldsymbol{\Gamma}_*) \;=\; \boldsymbol{\Delta t}^T \left(x_i \cdot \boldsymbol{\Gamma}_* (1 \,+\, \alpha\theta\overline{\gamma}) \,-\, \alpha\overline{\gamma}\Phi\left[x_i \cdot \boldsymbol{\Gamma}_*\right]\right) \;=\; \overline{\gamma}} \tag{3.45}$$

$$\boxed{(\boldsymbol{\Delta t} \circ \boldsymbol{\Gamma}_*)^T R'(x_i \cdot \boldsymbol{\Gamma}_*) \;=\; (\boldsymbol{\Delta t} \circ \boldsymbol{\Gamma}_*)^T \left(1 \,+\, \alpha\theta\overline{\gamma} - \alpha\overline{\gamma}\Phi'\left[x_i \cdot \boldsymbol{\Gamma}_*\right]\right) \;=\; 0} \tag{3.46}$$

with $\circ$ denoting the Hadamard product operator.

The following section is devoted to addressing the derivation of the second variation of J, given that, in previous works, it has been a great help during the resolution of VC problems.

3.3.2 Second variation analysis

We derive the expression for the second variation of J in order to evidence under what conditions the obtained solution is the extremal that maximizes the functional $\overline{\text{psr}}_*$.

We continue considering variations $v(t)$ over the SINR profile $\Gamma_*(t)$ and scalar variations δt_k over each free corner and end point t_k. For second order variations on $v(t)$ and δt_k, we take (3.19) and we expand it up to the second order, as follows,

$$\begin{aligned} \delta J\Big|_{\text{2nd}} \;&=\; \sum_{k=1}^{p} \int_{t_{k-1}}^{t_k} \left[\left(\frac{\partial F}{\partial \Gamma}\right) v(t) \;+\; \frac{1}{2}\left(\frac{\partial^2 F}{\partial \Gamma^2}\right) v^2(t)\right] \,\mathrm{d}t \\ &+\; \sum_{k=1}^{p} \left[\, F(t, \Gamma_*(t))\delta t \;+\; \left(\frac{\partial F}{\partial \Gamma}\right) v(t)\delta t \;+\; \frac{(\delta t)^2}{2} \nabla_t F(t, \Gamma_*(t)) \right]_{t_{k-1}^+}^{t_k^-} \end{aligned} \tag{3.47}$$

At the stationary point, we have that $\partial F/\partial \Gamma = 0$, that is, the first variation vanishes along with many second order cross-terms. Furthermore, in case of uniform channel gains we have that $\nabla_t F|_{\text{SP}} = 0$. Hence, we set $\delta J|_{\text{2nd}} \to \delta J|_{\text{2nd,SP}}$, and the second variation reduces to the following

$$\delta J\Big|_{\text{2nd,SP}} \;=\; \frac{1}{2} \sum_{k=1}^{p} \left(\frac{\partial^2 F_k}{\partial \Gamma^2}\right) \int_{t_{k-1}}^{t_k} v_{\text{SP}}^2(t) \,\mathrm{d}t \tag{3.48}$$

$$\frac{\partial^2 F_k}{\partial \Gamma^2} \;=\; \text{PSR}''[\Gamma_*^k] \;+\; \alpha\overline{\gamma} \sum_{i=0}^{M} \lambda_i \cdot x_i^2 \cdot \Phi''[x_i \cdot \Gamma_*^k] \tag{3.49}$$

with the k-th sub-index indicating the evaluation for the k-th piece of the solution profile and where the variations $v_{\text{SP}}(t)$ are subject to the admissible conditions (3.23) at the stationary point. At this point, the reader may notice that $\delta J|_{\text{2nd,SP}}$ only involves variations $v_{\text{SP}}^2(t)$ over the SINR profile. Therefore, a sufficient condition for ensuring that the multi-uniform profile maximizes $\overline{\text{psr}}_*$ is to set $\delta J|_{\text{2nd,SP}} < 0$, which must be verified for any $v_{\text{SP}}^2(t)$. Naturally, as $\int v_{\text{SP}}^2(t)\,\mathrm{d}t > 0$, the negativeness of (3.49) for all k is a sufficient condition to have a local maximizer. As (3.49) depends on the solution profile, it must be checked during the resolution procedure.

Nonetheless, we seek for an additional condition that allows us to predict the behaviour of the solution profiles. In Annex C, we derive that $\boxed{p \leq M + 1}$ must be verified in order to guarantee that the solution is not a saddle point. For several reasons the obtained inequality has become relevant during the work:

(i) The number of levels of the solution profile p is bounded by the number of FPs in f, $M + 1$.

(ii) Intuitively: every time a new level appears, 2 new degrees of freedom are needed to be solved (i.e. the level value and its interval length), which coincides with the 2 equations imposed by every active inequality (3.45 - 3.46).

3.3.3 Solution procedure

In the previous section, we showed that VC reduces the search of the optimum SINR to a multiuniform structure. Henceforth, we make use of classical optimization tools to address its resolution. There are two alternative ways of computing the solution of the former problem,

(i) Solving the system of equations constituted by the set of SPEs, TCs and constraints obtained from particularizing the derived equations of the VC problem for the case of constant channel gains.

In this case, we consider a discretization of the function $\lambda(x)$, comprised by the set of multipliers $\boldsymbol{\Lambda}$ at the positions $\boldsymbol{x}$ (see Section 3.2.2), and we make a summary of the number of unknowns to be determined (left) and the equations we have derived (right),

Unknowns		**Equations**	
SINR levels $\boldsymbol{\Gamma}_*$	$: p$	SPEs (3.39)	$: p$
User intervals $\boldsymbol{\Delta t}$	$: p+1$	TCs (3.40 − 3.41)	$: p$
Multipliers $\boldsymbol{\Lambda}$	$: M+1$	Constraints (3.44 − 3.46)	$: 2M+1$
$\{x_1, x_2, ..., x_M\}$	$: M$	$\mathbf{1}^T\boldsymbol{\Delta t} = 1$	$: 1$
Number of unknowns	$: 2p+2M+2$	Number of equations	$: 2p+2M+2$

The stated system constitutes a set of $2p+2M+2$ equations/unknowns that needs prior knowledge of the variables p and M.

However, the reader should note that there is no guarantee that any SINR solution profile verifying the previous system of equations will satisfy the constraints of the initial VC problem. In fact, as the function $\lambda(x)$ has been discretized, for every solution profile we found we must check if the initial constraint imposed by $\lambda(x)$ is met.

(ii) Solving the following discrete optimization problem, obtained from changing the integrals of the VC problem (3.13 - 3.15) for summations,

$$\max_{\boldsymbol{\Delta t},\, \boldsymbol{\Gamma}_*} \quad \overline{\text{psr}}_* = \boldsymbol{\Delta t}^T \text{PSR}\left[\boldsymbol{\Gamma}_*\right] \tag{3.50}$$

$$\text{s.t.} \quad \overline{\gamma} = \boldsymbol{\Delta t}^T R(\boldsymbol{\Gamma}_*) \tag{3.51}$$

$$\text{s.t.} \quad \overline{\gamma} \geq \boldsymbol{\Delta t}^T R(x \cdot \boldsymbol{\Gamma}_*) \quad 0 < x < 1 \tag{3.52}$$

$$\text{s.t.} \quad 1 = \mathbf{1}^T \boldsymbol{\Delta t} \tag{3.53}$$

$$\text{s.t.} \quad \boldsymbol{\Delta t} \geq \mathbf{0} \;,\; \boldsymbol{\Gamma}_* \geq \mathbf{0} \tag{3.54}$$

which constitutes a non-convex discrete optimization problem that needs prior knowledge of the number of levels p. Moreover, the reader should note that (3.52) constitutes an equation with a continuous set of constraints to enforce, which must be discretized in a finite but large set of inequality constraints.

Still, even in the uniform channel case and for an arbitrary combination of scenario parameters, the derived equations do not provide further information as to know how many pieces p the solution profile has, neither the number of tangencies M that are involved.

We have developed an own method that allows us to compute the optimal SINR profile in a more comfortable and easy way. The following section is devoted to explain the said algorithm.

3.3.4 Solution procedure. Incremental method

We are interested in designing an algorithm that allows the reader to reach the saturation point of the system as fast as possible. The described algorithm mixes both previous stated resolution methods.

Preliminaries

First, we will explain some steps which are necessary to understand the algorithm rationale.

The reader should note that, when the system works at very low load $\alpha \to 0$, no active inequality is set, and thus, the optimal SINR profile is uniform with $p = 1$ and $M = 0$.

We will propose an incremental method in the traffic load α that allows the computation of the SINR profile $\boldsymbol{\Gamma}_*, \boldsymbol{\Delta t}$ along with the required variables $\boldsymbol{\Lambda}, \boldsymbol{x}$ of the former problem. The underlying idea behind this incremental method is that solution profiles corresponding to closer traffic loads (α and $\alpha + \mathrm{d}\alpha$) are not substantially different. Naturally, this assumption is realistic in those regimes where the values of p and M are maintained. At those points where the optimum SINR profile needs an additional level or tangency, the solution may be drastically different, and hence, a more sophisticated search over the optimum values must be performed.

For simplicity during the rest of this section, we re-define the variables

$$\boldsymbol{\Gamma}_* \doteq [\, \Gamma_*^1 \ , \ \dots \ , \ \Gamma_*^p \,]^T \tag{3.55}$$

$$\boldsymbol{\Delta t} \doteq [\, \Delta t_1, \ \dots \ , \Delta t_p \,]^T \tag{3.56}$$

$$\boldsymbol{x} \doteq [\, x_1 \ , \ \dots \ , \ x_M \,]^T \tag{3.57}$$

where we have suppressed the last positions of $\boldsymbol{\Gamma}_*, \boldsymbol{\Delta t}$ and the first position of $\boldsymbol{x}$.

Under an initialization ($\boldsymbol{X}_0$) close enough to the optimum point, the discrete optimization problem in (3.50 - 3.54) results equivalent to the following

$$\max_{\boldsymbol{\Gamma}_*,\, \boldsymbol{\Delta t},\, \boldsymbol{x}} (\boldsymbol{X}_0) \qquad \boldsymbol{\Delta t}^T \mathrm{PSR}\,[\boldsymbol{\Gamma}_*] \tag{3.58}$$

$$\text{s.t.} \quad \overline{\gamma} = R\left[\boldsymbol{\Gamma}_*^T\right] \boldsymbol{\Delta t} \tag{3.59}$$

$$\text{s.t.} \quad \overline{\gamma} \cdot \mathbf{1} = R\left[\, \boldsymbol{x} \cdot \boldsymbol{\Gamma}_*^T \,\right] \boldsymbol{\Delta t} \tag{3.60}$$

$$\text{s.t.} \quad \mathbf{0} = R'\left[\, \boldsymbol{x} \cdot \boldsymbol{\Gamma}_*^T \,\right] (\boldsymbol{\Gamma}_* \circ \boldsymbol{\Delta t}) \tag{3.61}$$

$$\text{s.t.} \quad 1 = \mathbf{1}^T \boldsymbol{\Delta t} \tag{3.62}$$

$$\text{s.t.} \quad \boldsymbol{\Delta t} \geq \mathbf{0} \ , \ \boldsymbol{\Gamma}_* \geq \mathbf{0} \ , \ \boldsymbol{x} \geq \mathbf{0} \ , \ \boldsymbol{x} \leq \mathbf{1} \tag{3.63}$$

where we have discretized the set of infinite inequalities (3.52) into $2M$ equality constraints (3.60 - 3.61). It should be highlighted that the solution of this discrete optimization problem corresponds to the closest optimum to $\boldsymbol{X}_0$.

Description of the incremental algorithm

Let $\mathcal{X}(\alpha) = \{\alpha, \overline{E}, N_0, \mathrm{PER}[\Gamma], \Phi[\Gamma]\}$ be the set of parameters of the considered scenario for which we want to compute its optimal SINR profile, with α the system's traffic load. Let α_0 be a traffic load for which the uniform SINR profile optimizes the stated problem for the parameter set $\mathcal{X}(\alpha_0)$.

Let us start the algorithm with α_0, traffic load for which the optimum SINR profile is known, i.e. uniform SINR profile. From this known profile, the next step is to increase the traffic load by $\alpha + \mathrm{d}\alpha$ and solve the discrete optimization problem (3.58 - 3.63) using as initialization seed the obtained solution for the previous iteration (α_0). For sufficiently small $\mathrm{d}\alpha$, the solution profiles from consecutive loads will not differ too much. Thus, the proposed initialization results in a intelligent way to counteract the ignorance of the variables that involve the optimum profile. The following lines are dedicated to detail the proposed iterative algorithm,

(i) At the 0th iteration ($i = 0$), consider the initial traffic load α_0 and initialize $p = 1$ and $M = 0$. Using the energy profile $E_{\mathrm{r}}(t) = \overline{E}$ for $0 < t \leq 1$, compute the interference level ξ_* from $\xi_* = f(\xi_*)$.

(ii) Define the initialization point for the 1st iteration $\boldsymbol{X}_0$, as the concatenation of $\boldsymbol{\Gamma}_* = [\, \overline{E}/(N_0 + \xi_*) \,]$, $\boldsymbol{\Delta t} = [\, 1 \,]$ and $\boldsymbol{x} = [\,]$.

(iii) Update variables $\alpha \to \alpha + \mathrm{d}\alpha$ and $i \to i + 1$.

(iv) Solve the discrete optimization (3.58 - 3.63) problem using the initialization seed $\boldsymbol{X}_0$.

(v) Compute $\boldsymbol{\Lambda}$ from the SPE and WE TCs and check constraints of the VC problem.

(vi) If the constraints are:

  (a) OK: Save results. Update the initialization point $\boldsymbol{X}_0$ with the obtained optimum variables $\boldsymbol{\Gamma}_*, \boldsymbol{\Delta t}, \boldsymbol{x}$. Return to (iii).

  (b) Not OK: Analyse results computing $\int R \, \mathrm{d}t$ for $0 < x < 1$.

    (i) If a new tangency appears:
    Set $M \to M + 1$ and $p \to p + 1$.
    Modify the used initialization point in order to include the new variables.
    Return to (iv).

    (ii) The system has reach its saturation point (Enable user admission index $t_p < 1$).
    Set $p \to p + 1$. Modify the used initialization point in order to include the new variables.
    Return to (iv).

The reader should note that, in fact, when a new tangency is set, it does not imply that a new level should be activated. Nonetheless, we decided to set the new level in order to include an additional degree of freedom, allowing the algorithm to use it when the time is right.

In fact, in this section we make use of the knowledge obtained during the simulations, where it is highlighted that profiles with higher levels provide better performances. However, to reach local optima, it is not necessary to include a new level in the point where a new tangency appears, step (vi.b.i) in the algorithm.

Chapter 4

Simulations and Results

As the derived asymptotic expressions in Chapter 3 depend on the considered FEC code, we have evaluated the performance of the proposed PMDF scheme for two representative FEC codes of rate $R_c = 1/2$:

(a) The classical convolutional code (CC) with constraint length $\mathcal{K} = 7$ and generator polynomials 133_{oct} and 171_{oct} adopted in the standards DVB-S [38] or IEEE 802.11 [39] with soft symbol decisions.

(b) The quasi-cyclic Low-Density Parity-Check (LDPC) code of the DVB-S2 standard [40].

The LDPC is selected as example of an abrupt PER[Γ] curve whereas the CC is used to evaluate the performance of the proposed scheme for a smoother PER[Γ] curve. Anyhow, the results in this section can be repeated for any modulation and coding scheme as long as perfect knowledge of its PER curve is available. Figure 4.1 depicts the PER[Γ] (left) and PSR[Γ] (right) curves of both aforesaid codes, which we use as lookup tables instead of performing the real encoding and decoding processes.

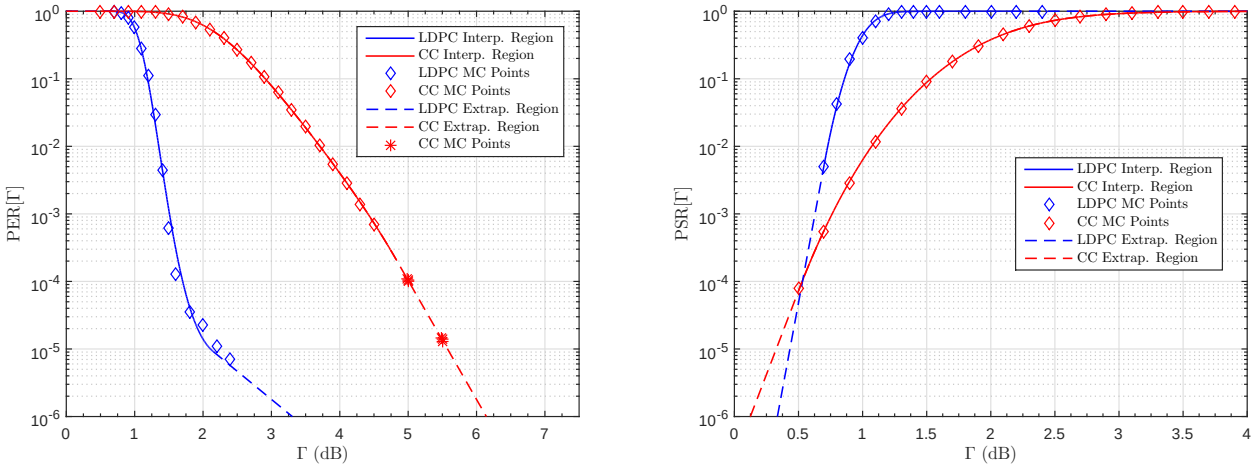

Figure 4.1: PER[Γ] and PSR[Γ] curves of the LDPC (blue) and CC (red) codes.

Diamond markers denote the simulated Monte Carlo points corresponding to the LDPC (blue) and CC (red) codes. In continuous line, we show the interpolated PER[Γ] and PSR[Γ] = 1 − PER[Γ] curves within the region defined by the simulated Γ-points, while dashed lines indicate their linearly log-extrapolated regions. For the CC, asterisks show further Monte Carlo simulations that validate the extrapolation. Small discrepancies appear for the LDPC while a negligible mismatching between both the Monte Carlo and the interpolated/extrapolated models is evidenced for the CC. However, at the extrapolated regions, notorious dissimilarities would appear for increasing Γ, and thus, exact PER and PSR values should only be assumed true within the simulated Γ points. Anyway, we decided to use the present models given that their derivatives result well defined (see Appendix E for further clarifications).

4.1 User-asymptotic simulations

We have evaluated the asymptotic theoretical expressions for a representative scenario under uniform channel gains $h(t) = 1$ that follows the described system model in Chapter 2. We consider QPSK-modulated spread-spectrum users transmitting with a shaping pulse of roll-off factor $\beta = 0$[1] and an average EsNo $\overline{\gamma} = 15$ dB. At the decoder, for lack of knowledge of the residual interference power function $\epsilon(\Gamma)$, we will assume it independent of Γ, with $\epsilon(\Gamma) = 0.1$, and the decorrelation factor is set to $\theta = 1$.

4.1.1 Spectral efficiency and average system's PER over all users

We depict in Figure 4.2 the average spectral efficiency over all users for the computed optimal profiles and for both described codes. Also, in order to evidence the benefit of the studied PMDF scheme, we have evaluated the correlator bank introduced in Appendix F (black line).

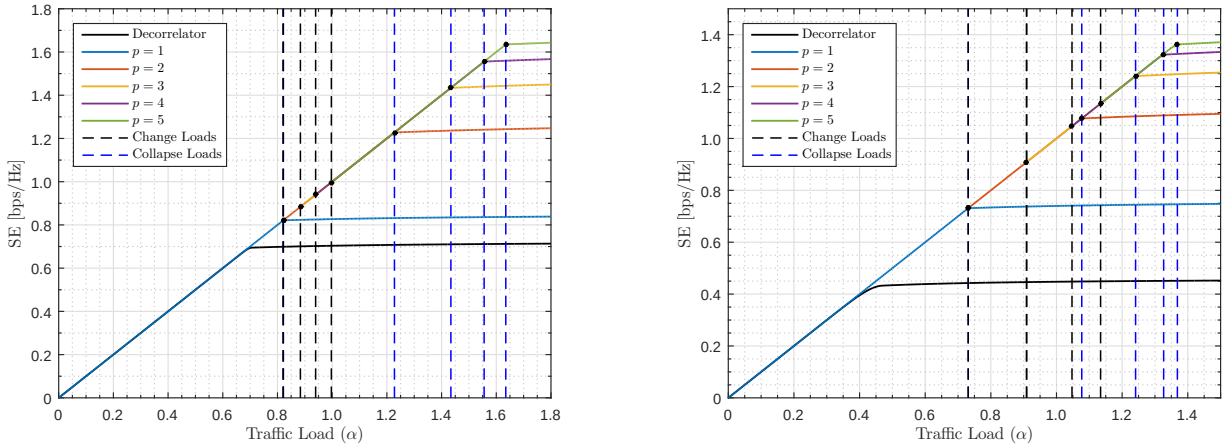

Figure 4.2: Spectral efficiency vs. traffic load α for the LDPC (left) and the CC (right) codes. Dashed lines indicate the critical loads from which: an additional energy level is appended (*change loads*) or the user admission index is enabled, while maintaining the number of non-zero energy levels (*collapse loads*). For $p = 1$, both the change and the collapse loads coincide.

The continuous blue line illustrates the spectral efficiency achieved with a single energy level, which coincides with the extremal that maximizes the system's performance in the space of continuous functions with a user admission index. In our considered space $\mathcal{D}$, the throughput of the system is significantly improved by introducing more levels into the ordered energy distribution. For both simulated codes, the first level ($p = 1$) is maintained until it collapses. Contrarily, for the rest of levels it is convenient to switch to a profile with one more level before they collapse.

For the sake of simplicity, we stopped the simulations at $p = 5$ for both the LDPC and the CC codes, but more levels are expected for increasing loads. As expected, since the LDPC is more powerful than the CC, it accepts more load for the same number of levels. For the performed simulations, the maximum accepted load for each code is $\alpha = 1.6348$ and $\alpha = 1.3684$, respectively. In both cases, the spectral efficiency exceeds 1 bps/Hz, the theoretical limit value for orthogonal multiple access.

Moreover, it should be noted that the throughput maximization problem resulted in an optimization task with multiple solutions (multimodal). In that respect, as to evidence the discrepancies between the different optima, we illustrate in Figure 4.3 the average PER over all users at the FP ξ_*, $\overline{\text{per}}_* = 1 - \overline{\text{psr}}_*$, for the computed optimal profiles and for both described codes.

[1] The selection of the roll-off factor results in a proportionality factor over the spectral efficiency. The chosen value does not correspond to a practical case, but it has been chosen in order to simplify the interpretation of the results.

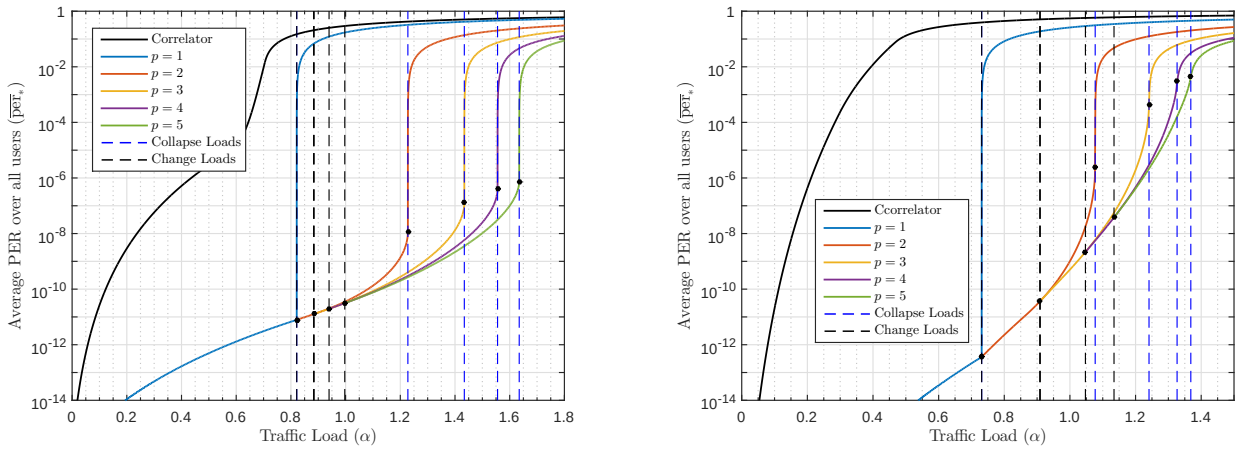

Figure 4.3: Average PER over all users vs. traffic load α for the LDPC (left) and the CC (right) codes.

For those traffic loads in which many extremal functions appear, the absolute optimum corresponds to the profile with more levels. Nevertheless, near the change loads (black dashed lines), there is an insignificant performance degradation when considering local optima with a lower but close number of levels than the profile associated with the absolute optimum point.

4.1.2 Optimum EsNo profiles

In this Section, we present the optimum EsNo profiles as a function of the traffic load. For a better understanding, we divide this section in two main parts. First, we only depict the values associated with the absolute optimum solution profiles, for later on evidence their evolution for the local optimum cases.

Absolute optimum EsNo profiles

We detail in Figures 4.4 and 4.5 the evolution of the absolute optimal EsNo levels and their associated user intervals, respectively, as a function of the traffic load.

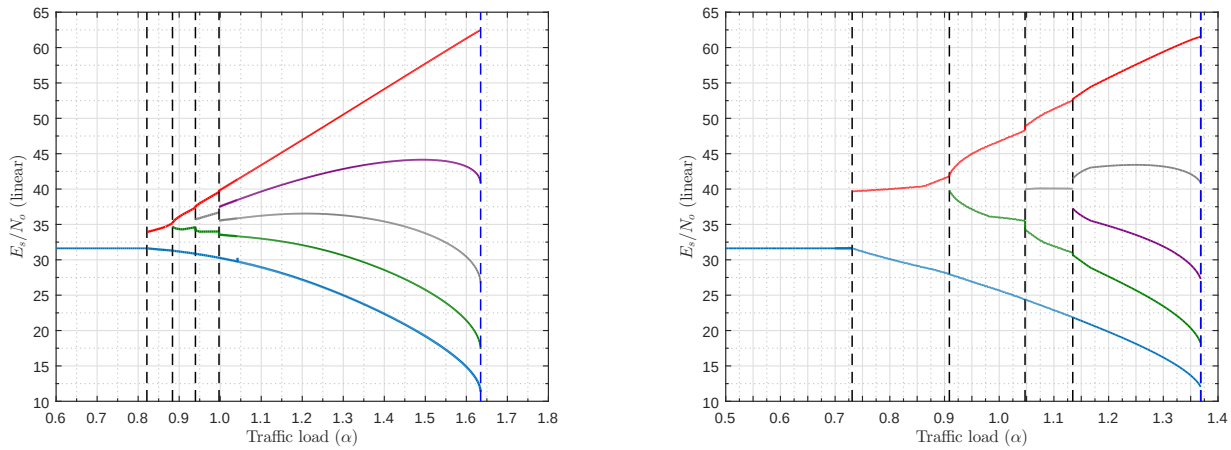

Figure 4.4: Absolute optimum EsNo levels vs. traffic load α for the LDPC (left) and the CC (right) codes.

At every change load, a new level appears from the first or second strongest EsNo level. At these loads, the magnitude of the imbalance between levels is lessened the more abrupt the PER curve of the used FEC code is. The lowest EsNo level continuously decreases as the load increases. Near the collapse load

of $p = 5$ (blue dashed line), all the EsNo levels, except the strongest one (red line), fall asymptotically to zero unless the admission user index is enabled.

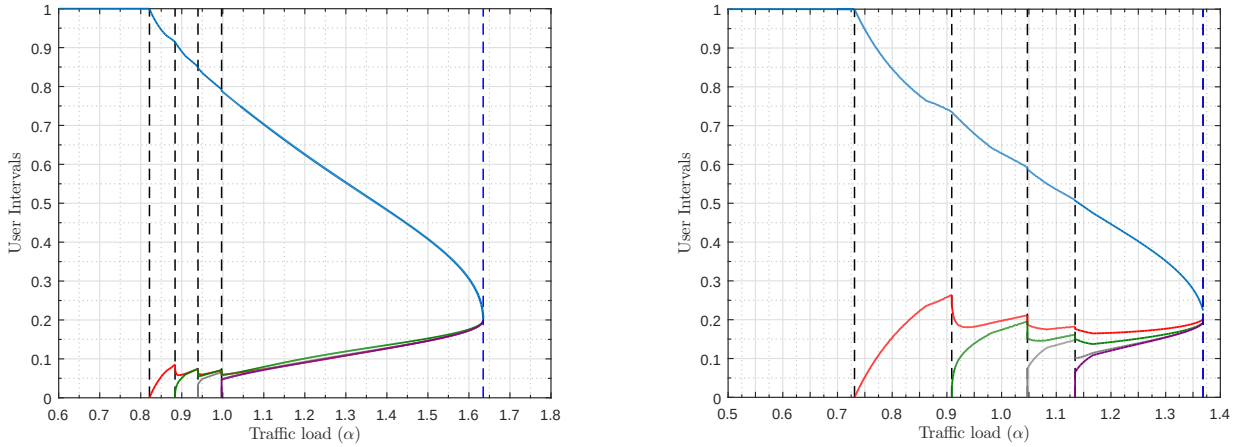

Figure 4.5: Absolute optimum user intervals vs. traffic load α for the LDPC (left) and the CC (right) codes.

As a general rule, the new EsNo levels are incorporated with few users contained in them, and keep increasing their lengths while the traffic load increases. Moreover, for FEC codes with abrupt PER curves, the new incorporated levels that appear present similar user intervals (e.g. for $\alpha = 1.5$ we have $\Delta t_1 \approx \cdots \approx \Delta t_4 \approx 0.15$ and $\Delta t_5 \approx 0.4$); such that, in practice two different interval values appear. Additionally, the lowest EsNo level is the one containing the higher fraction of users. For the simulated cases, the collapse load of $p = 5$ corresponds to the case in which its EsNo levels are equally distributed over the user ordering, that is, $\Delta t_1 = \cdots = \Delta t_5 = 0.2$.

Local optimum EsNo profiles

Over the previous figures, we also depict in dashed lines, the EsNo values corresponding to the local optimum profiles, that is, the profiles resulting of not appending additional levels, at the change loads, over the user ordering.

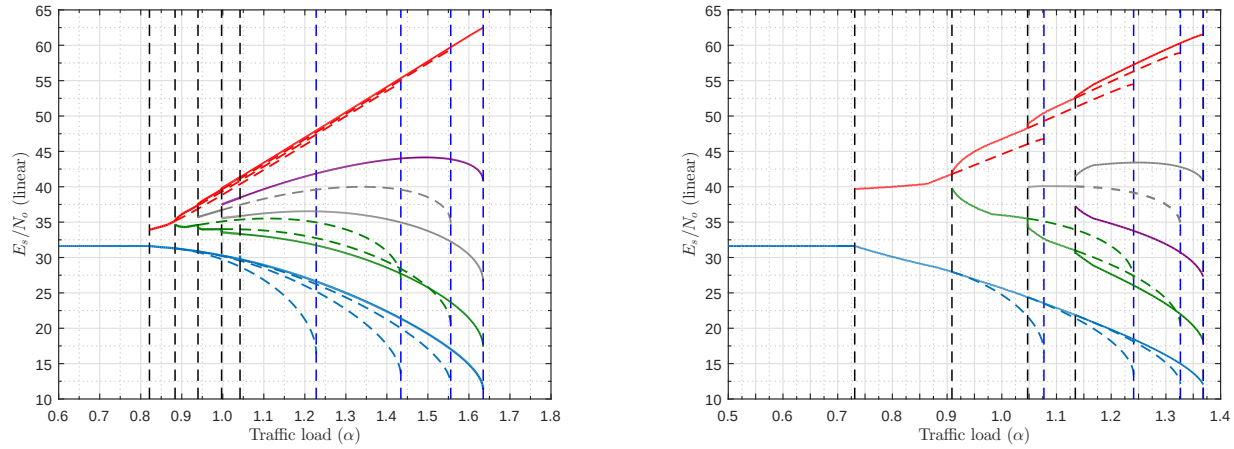

Figure 4.6: EsNo levels vs. traffic load α for the LDPC (left) and the CC (right) codes.

At the collapse loads, lower energy levels fall asymptotically to zero unless the admission user index is enabled. It should be remarked that, due to this asymptotic behaviour, the determination of the optimal profiles turned out very difficult since strong numerical issues appeared.

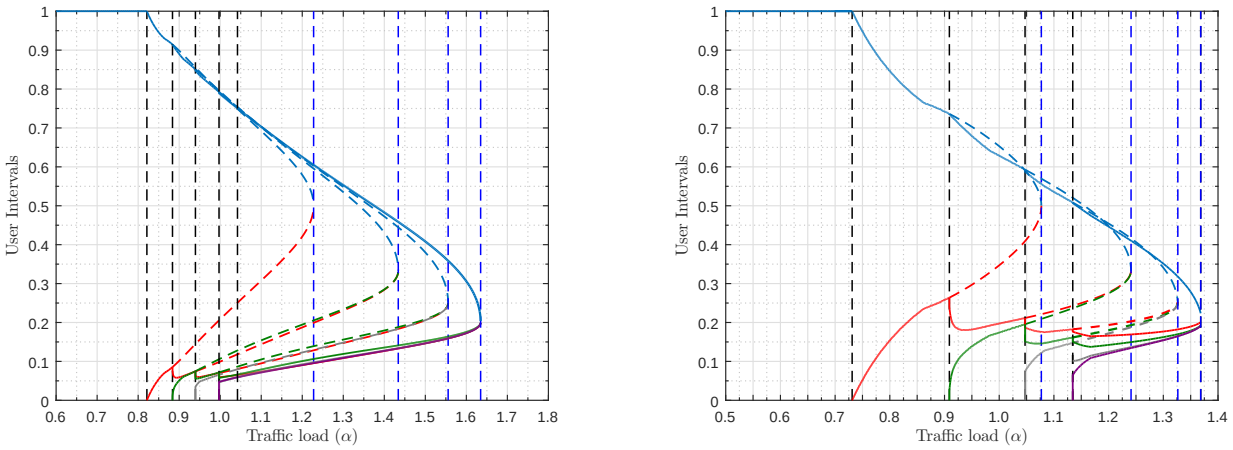

Figure 4.7: User intervals vs. traffic load α for the LDPC (left) and the CC (right) codes.

In these local optimum profiles, the user interval corresponding to the lowest energy level decreases while, in general, the rest of intervals increase until they collapse. The collapse load of each profile occurs when their levels are equally distributed over the user ordering, e.g. for $p = 2$ we have that $\Delta t_1 = \Delta t_2 = 0.5$.

Monte Carlo simulations

We have validated the results of the discrete non-linear optimization by evaluating the asymptotic expressions for random generated multi-uniform energy profiles and by computing between 10^8 - 10^9 Monte Carlo simulations for each traffic load.

In that respect, the dimensionality of the searching space is $2p - 2$ ($2p$ degrees of freedom for each profile and 2 equations (energy constraint and user interval length)). For the low dimensionality cases, we show in Figures 4.8 and 4.9 the Monte Carlo points depicted as diamond markers over the previous Figures 4.6 and 4.7.

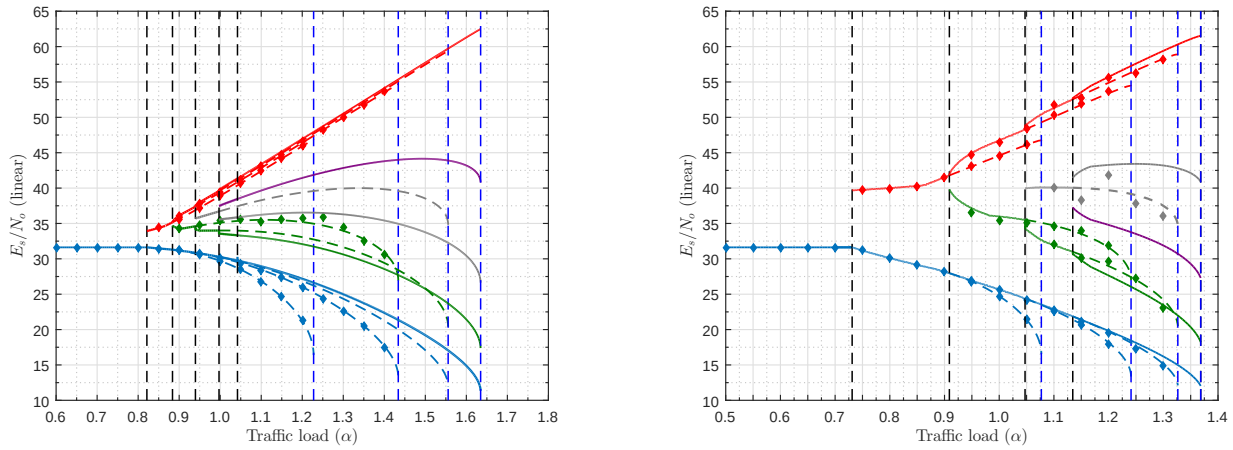

Figure 4.8: EsNo levels vs. traffic load α for the LDPC (left) and the CC (right) codes. Monte Carlo simulations.

Results show the matching between both the discrete optimization and the Monte Carlo simulations, and highlight the benefit of using the proposed incremental algorithm described in Section 3.3.4 at the cost of computing the optimal profiles associated with the preceding traffic loads.

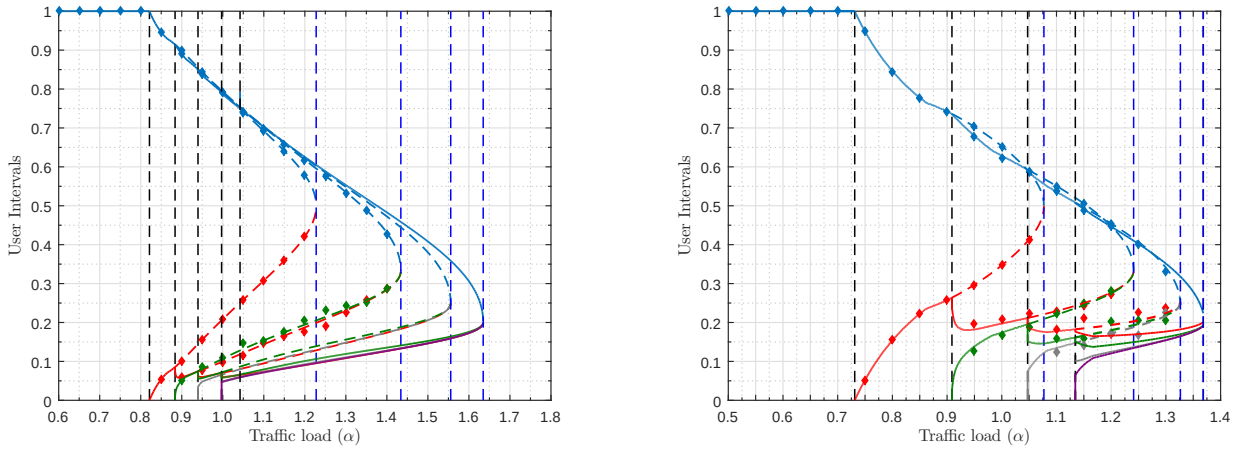

Figure 4.9: User intervals vs. traffic load α for the LDPC (left) and the CC (right) codes. Monte Carlo simulations.

4.1.3 Optimum SINR profiles

As the SINR level values are also relevant for the evaluated expressions, we depict in Figure 4.10 the values of the optimum SINR profiles at the FP ξ_*.

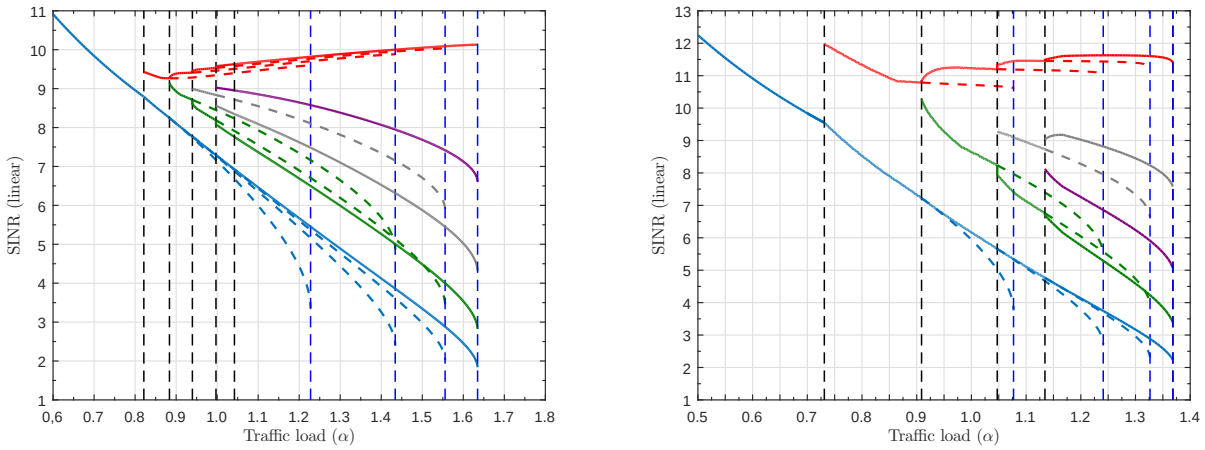

Figure 4.10: SINR levels vs. traffic load α for the LDPC (left) and the CC (right) codes.

As a general rule, it is beneficial to decrease the values of the lower SINR levels as the load increases. On the contrary, stronger users (red line) are able to practically maintain their SINR levels or even increase them. In particular, for both codes and $p \geq 3$, the strongest SINR level (red line) is increased with every new appended level.

4.1.4 Evolution of the number of levels p and the tangencies M

As we are interested in evidencing whether the obtained solution maximizes the functional $\overline{\text{psr}}_*$ according to the derived expressions in Section 3.3.2, we depict in Figure 4.11 the evolution of the variables $\{p, M\}$ as the traffic load increases.

We show the achievable region, which describes where the inequality $p \leq M + 1$ is satisfied. That is, inside this shadow region, the multiuniform function obtained in Section 3.2 maximizes $\overline{\text{psr}}_*$.

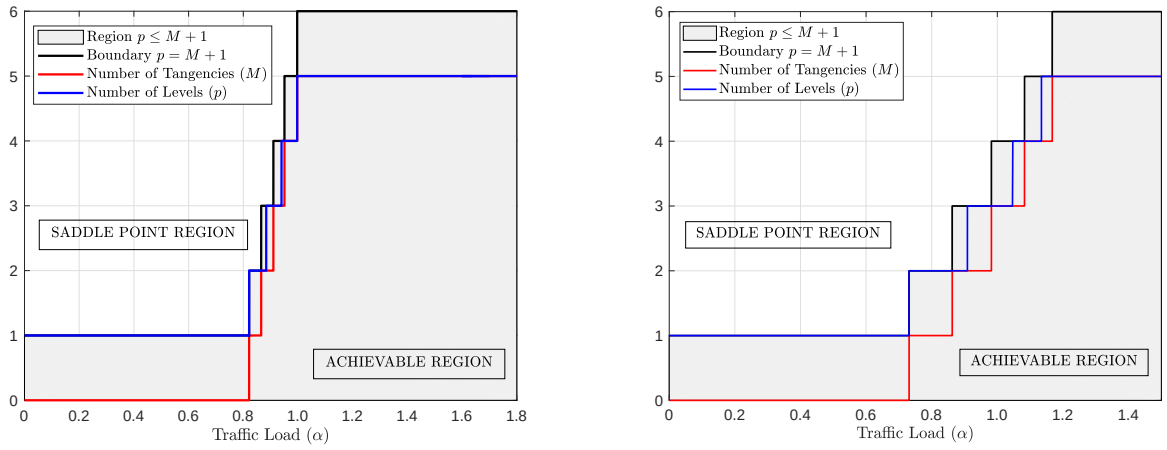

Figure 4.11: Evolution of p and M vs. traffic load α for the LDPC (left) and the CC (right) codes.

As can be seen in Figure 4.11, the behaviour of the first level is different when compared with the other ones. For the uniform profile ($p = 1$), once the first tangency appears, it is convenient to change to a profile with two levels. This is because the uniform profile does not have any degree of freedom to force that f does not exceed the ξ line. In any other case, once a new tangency appears it is worth maintaining the same number of levels during a certain amount of load. After that, it is beneficial to introduce a new level into the users profile. Moreover, the mentioned amount of traffic load is reduced the more abrupt the PER curve of the used FEC code is.

4.1.5 Dependence with the average transmitted EsNo

In Section 4.1.1, we showed the average PER over all users when using two different codes while maintaining the same working EsNo $\overline{\gamma} = 15$ dB. This section is devoted to illustrating the deviation of the system's performance, in terms of average PER, with the working average transmitted EsNo $\overline{\gamma}$, which for simplicity it is only presented for the CC.

We have evaluated the asymptotic equations for different $\overline{\gamma}$ values. In particular, we depict in Figure 4.12 the average PER over all users at the FP ξ_* for the average EsNo values: $\overline{\gamma} = \{10, 15, 20\}$ dB.

As the average EsNo $\overline{\gamma}$ increases, the profiles with the same number of levels are able to accept more traffic load before appending a new level. In other words, the collapse loads are displaced towards increasing loads. These movements are more notorious the more levels the target profiles have, e.g. at the change load from 1 to 2 levels, the difference between collapse loads of 10dB and 20dB is $\Delta\alpha \approx 0.10$ while in the change load from 4 to 5 levels is $\Delta\alpha \approx 0.16$.

Additionally, in terms of average PER, it can be seen that the shape of the depicted curves is the same but they are displaced along the y-axis.

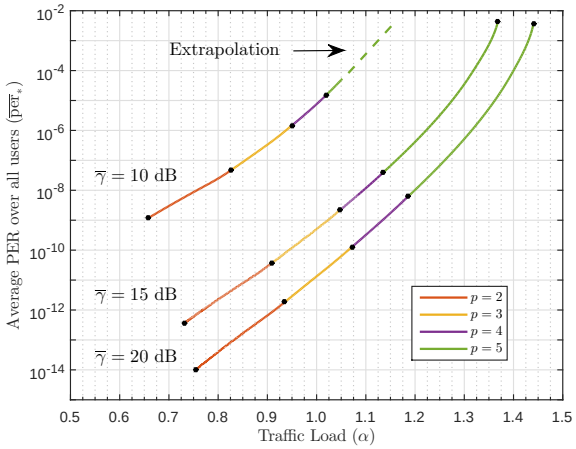

Figure 4.12: Average PER vs. traffic load α for the CC and different $\overline{\gamma}$ values.

For the same increment in $\overline{\gamma}$, a significant performance improvement is experimented for moderate $\overline{\gamma}$ values (10dB) while, for high EsNo values (15dB), this gain is reduced.

4.1.6 Dependence with the δ constriction

This section is dedicated to showing the dependence of the system's performance as a function of the tunnel width δ. For simplicity, we will only evaluate this section for the CC and the same EsNo profile, the one associated with the collapse load of 2 levels ($\alpha = 1.077$), since the obtained results can be easily extrapolated for any considered profile.

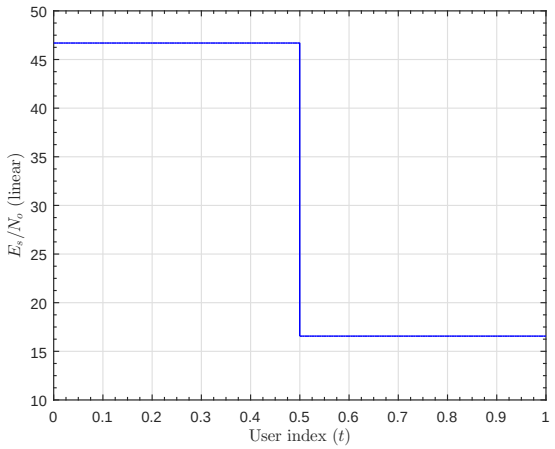

Figure 4.13: Collapse EsNo profile of 2 levels for the CC computed with $\delta = 0$.

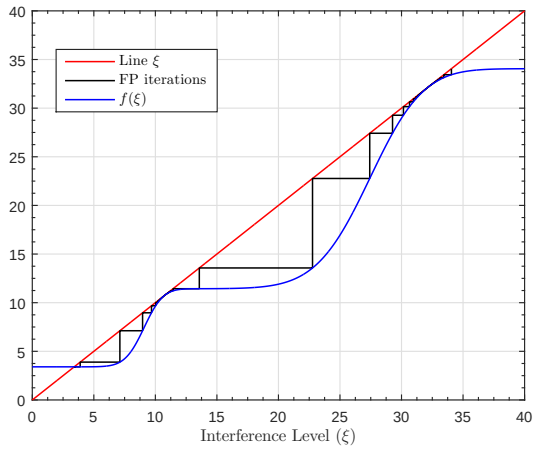

Figure 4.14: Function f that generates the collapse EsNo profile of 2 levels for the CC with $\delta = 1 \cdot 10^{-4}$.

We also show in Figure 4.15, the evolution, throughout DF stages i, of the common MAI level ξ_i (left) and its associated average PER over all users (right).

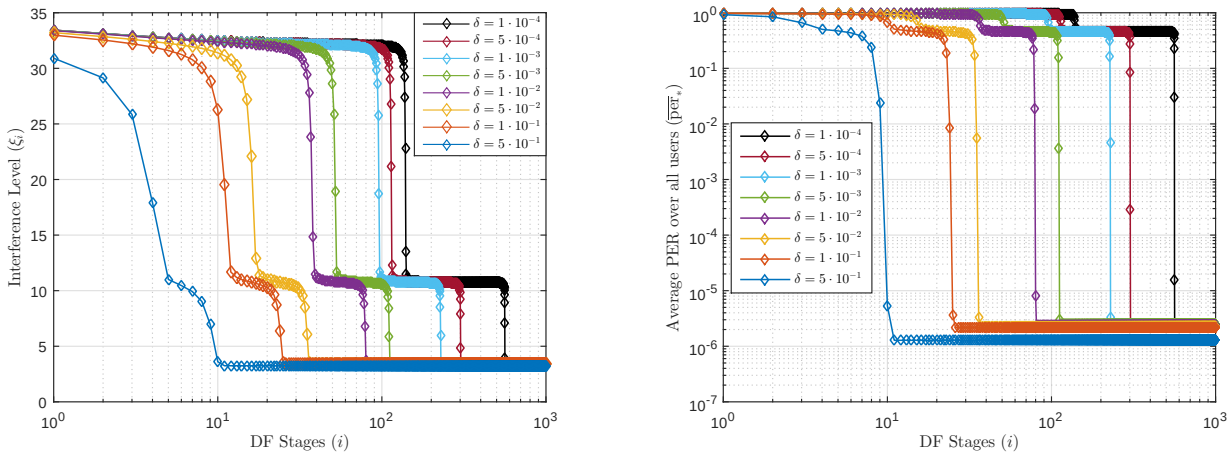

Figure 4.15: Interference level (left) and average PER (right) throughout DF stages (i) for different δ values.

The system performs more iterations at the regions in which it crosses each one of the tunnels. The common MAI level is practically static over small changes on δ (see the left part of Figure 4.15) while the number of DF stages necessary to get the FP is significantly reduced. For the simulated cases, the overall PER suffers from negligible deviations. Nonetheless, these deviations may depend on the working point at the PER curve at which the system works.

An increase of the δ parameter results in an improvement of the average PER, but it must be remarked that it is the consequence of a reduction in the traffic load. The present load imbalance is only optimal when an infinitesimal reduction is performed and the system's latency is not constrained. Otherwise, in case of latency constrained systems, it is worth to reformulate and solve the stated VC problem by introducing a function $g(\xi)$ in order to open the tunnels.

4.1.7 Evolution of the optimal profiles

This section is completely devoted to showing the evolution of the optimum EsNo profiles and the interference function, f, they generate as the traffic load increases. This section may be of interest given that the proposed algorithm in Section 3.3.4 is based on the similarity assumption between solutions corresponding to closer traffic loads.

In the following figures, we depict the mentioned evolution, that, for simplicity, is only presented for the CC. In particular, in all the subsequent figures, three profile examples with the same number of levels are illustrated. They correspond to three different traffic loads: first, near the change load; second, after a new tangency appears; and finally, at the collapse load. The absolute optimum profiles are shown in continuous lines while the local optimum ones are depicted in dashed lines.

Anyway, any reader may be free to infer the major part of the subsequent rationales, extracted from the CC, for any code in order to predict the evolution of its optimum functions as the traffic load increases.

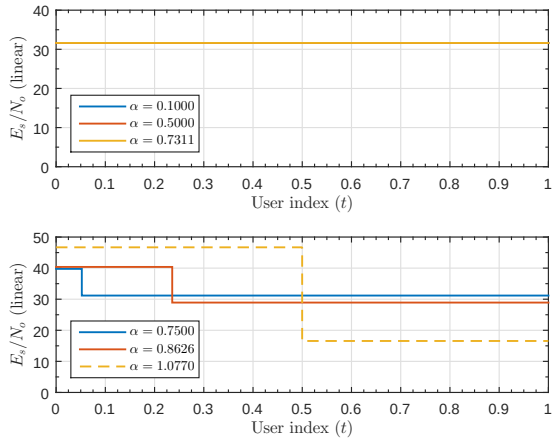

Figure 4.16: Optimum EsNo profiles of 1 (above) and 2 (below) levels for three traffic load values.

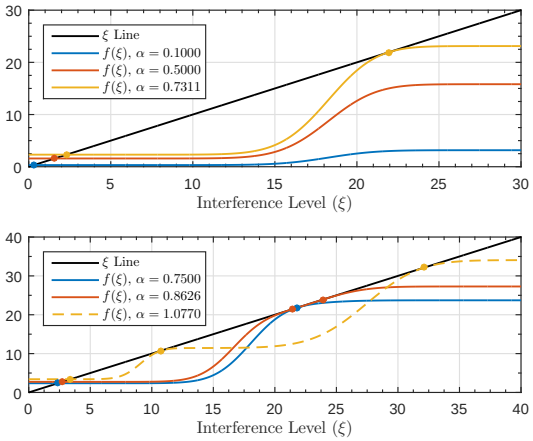

Figure 4.17: Function f that generate the depicted profiles of 1 (above) and 2 (below) levels.

For low traffic loads, the optimum profiles are uniform (see the upper part of Figure 4.16, where the three profiles are overlapped). The interference function that this profile generates for very low traffic loads (e.g. $\alpha = 0.1000$, blue line) is practically flat over the variable ξ, as depicted in the upper part of Figure 4.17. As the traffic load increases, f (red line) gets closer to the ξ line (black line) until they are tangent (yellow line).

The natural tendency of the function f, as the traffic load increases, is to surpass the ξ line, which would not satisfy the constraints of the stated VC problem in Section 3.2. Therefore, the load $\alpha = 0.7311$ becomes the collapse load of the uniform profile, and hereupon, a new inequality multiplier is activated, which sets a tangency such that the constraints imposed over the stated VC problem are verified.

As depicted in the lower part of Figures 4.16 and 4.17, near the change regions between 1 and 2 EsNo levels ($\alpha = 0.7500$), it is beneficial to convert the uniform profile into a bi-uniform one. This profile contains a high EsNo level with few users whereas the rest of the users are allocated to a lower EsNo value (blue line). As shown in the lower part of Figure 4.17, a single tangency is hold (blue line). For subsequent traffic loads, it is convenient to modify the prior profile by adding more users into the strong EsNo level. At the load $\alpha = 0.8626$ (red line) a new tangency appears, and thus, another inequality multiplier is activated in order to fulfil the constraints over the stated VC problem.

At this point, two options appear: (i) continue with $p = 2$, or, (ii) set $p = 3$. In the first case, the highest EsNo level continues increasing its value along with the fraction of users that it contains. On the

contrary, the lowest EsNo level decreases its value as well as its number of users. The stated behaviour is preserved until both levels are equally distributed over the user ordering i.e. $\Delta t_1 = \Delta t_2 = 0.5$ (yellow line). Regarding the interference function f, both tangencies are moved over the ξ line in opposite directions (see the lower part of Figure 4.17). Further from this collapse load, the user admission index should be enabled in order not to degrade the system's performance. However, after the new tangency appears, it seems beneficial to introduce a new level into the ordered energy distribution as stated in previous sections. In fact, during a certain amount of load, the new appended level is set equal to one of the previous levels, meaning that only 2 levels are necessary. Later, the last introduced level is imbalanced from the others resulting in a tri-uniform profile.

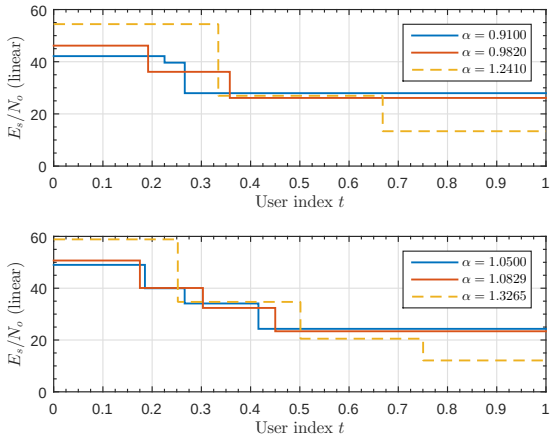

Figure 4.18: Optimum EsNo profiles of 3 (above) and 4 (below) levels for three traffic load values.

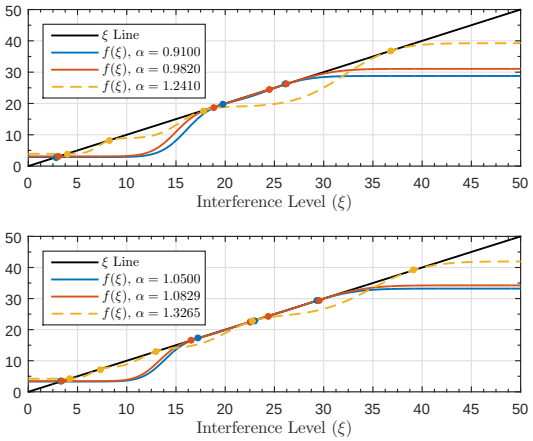

Figure 4.19: Interference function f that generate the depicted profiles for three traffic load values.

As illustrated in the upper part of Figure 4.18, the first tri-uniform profile does not follow the same behaviour when compared with the initial bi-uniform profile in Figure 4.16. In this case, it is convenient to append a new energy level between both previous levels with few users comprising in it (blue line). The interference function that generates such a profile has $M = 2$ tangencies (see the blue line on the upper part of Figure 4.19). Regarding the EsNo levels, the first level increases while the rest of levels decrease. For the new energy level, its user interval increases while it decreases for the rest of the levels (blue line).

This behaviour is maintained until a new tangency, between the previous ones, appears (red line). Again, we set a new inequality multiplier and, from here, two options arise: (i) continue with $p = 3$; (ii) set $p = 4$. In the first case, the first level increases its EsNo level while the second and the third one decrease theirs. Moreover, the lengths of the two highest EsNo levels keep increasing whereas the length of the lowest one decreases until they are equally distributed i.e. $\Delta t_1 = \Delta t_2 = \Delta t_3 = 1/3$ (see the yellow line on the upper part of Figure 4.19). As far as the tangencies are concerned, the tangency with greater interference level is moved towards increasing positions while the other ones decrease their positions.

As depicted in the lower part of Figure 4.18, in case of $p = 4$ (blue line), the new appended level has the second greatest EsNo level. Before the new tangency appears, its EsNo levels remain practically static although the highest and lowest EsNo levels experiment a slight increase and decrease, respectively. The user intervals of the first and last level decrease while the intermediate ones increase. Once the new tangency appears (red line), the highest EsNo level increases while the rest of ones decrease, and their intervals increase, except the last one, until they are equally distributed (yellow line).

In Figure 4.20, we present the optimum EsNo profiles for $p = 5$ levels (above) and the interference function that they generatee (below). In this case, the new EsNo level appears the third level into the ordered distribution with few users comprised therein (blue line). As the traffic load increases, the first 2 levels increase their EsNo values while diminishing their user intervals. On the contrary, the rest of levels decrease their EsNo values and increase their lengths except the lower level, which decreases its user interval (red line). Again, after a new tangency appears, the optimum EsNo profile evolves until their levels are equally distributed over the user ordering i.e. $\Delta t_1 = \cdots = \Delta t_5 = 0.2$.

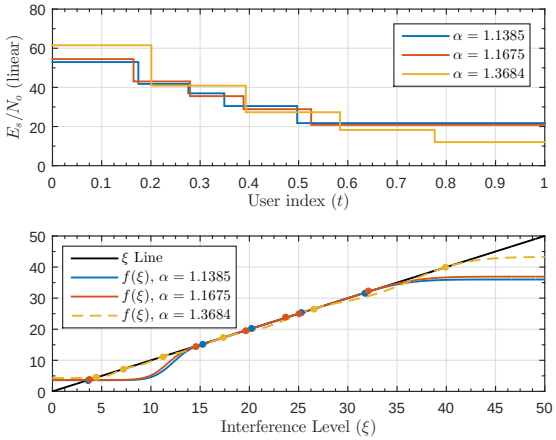

Figure 4.20: Optimum EsNo profiles of 5 levels (above) and the interference function f they generate (below) for three traffic load values.

To conclude this section, we summarize the main contributions evidenced during the evolution of the optimal EsNo profiles:

(i) The uniform profile is held until it collapses while the rest of profiles are changed after a new tangency appears.

(ii) Every time a new level is appended, it is worth introducing few users.

(iii) Before a new tangency appears, the profiles evolve in such a way that, the highest EsNo level increases and the lowest one decreases. Their user intervals progress depending on the number of levels p of the optimum profile.

(iv) Tangencies are shifted along the ξ line as the traffic load variates.

(v) Local optimum profiles can be maintained until their levels are equally distributed over the user ordering.

Chapter 5

Conclusions and Future Work

In this thesis, we have investigated the throughput maximization of a dense multiple access network of low-rate and energy-limited users sharing the same FEC code and whose central node implements a parallel multistage decision-feedback scheme for MAI mitigation. In the user-asymptotic case, we have employed VC techniques for determining the optimum energy allocation function that maximizes the spectral efficiency of such a multiple access network when user transmissions are constrained to fulfil a long-term per-user average energy constraint. This constitutes a scenario of interest for massive wide area M2M communications, currently an area of active research.

Although VC provides valuable tools for addressing the optimization of global utilities over a space of functions (e.g. aggregate packet error rate), it has been seldom applied in communication contexts. In this respect, massive multiple access has revealed itself a specially suitable field. Therefore, in contrast with related problems in the literature on massive IC receivers, our main contribution has been to adopt the more general class of piecewise continuous (discontinuous) energy profiles or energy allocation functions as candidates to fulfil the stated VC problem. This has brought to light the possibility of considering such functions (also known as broken extremal solutions) in other VC problems related with IC.

For a proof-of-concept scenario with uniform channel gains, we have shown that the optimal energy profile (i.e. the distribution of ordered energies) has the structure of a multi-uniform function. Hence, the throughput of the network is significantly improved by introducing more levels into the optimum energy distribution as the system's traffic load increases. In fact, we have proved through simulations that energy profiles with a higher number of levels achieve better performances. In the mathematical terms of the work, these profiles generate an interference function $f(\xi)$ that has M tangencies with the identity function $g(\xi) = \xi$ (the so-called ξ line). New levels are incorporated to the ordered energy distribution as new tangencies appear. Empirically, we have shown that the number of levels p of the optimum profile is, in fact, bounded by $M \leq p \leq M + 1$.

In somewhat more detail, the collapse of the first energy level has been found to coincide exactly with the appearance of the first tangency. From this point onwards, the change loads do not coincide with the occurrence of a new tangency. In fact, once the new tangency is set, it is beneficial to maintain the same number of levels over an interval of traffic loads. A new level is thereafter appended to the optimum energy distribution, improving the performance of the prior profile. New levels contain comparatively fewer users (in the asymptotic sense) and appear between the highest levels. Their imbalance with respect to the other levels is reduced as the PER curve becomes more abrupt. Moreover, their user intervals keep growing as the traffic load increases. In fact, we have shown that local optimum profiles with a fixed number of levels can be maintained until their levels are equally distributed over the user ordering. Intensive Monte Carlo simulations have allowed us to validate the obtained results.

Finally, we have shown that the system's latency is conditioned by the tunnels' widths, a feature related with the smallest gaps between the interference function $f(\xi)$ and the ξ line. For the proposed method, we have illustrated that the number of decision-feedback stages needed to pass the tunnels is very sensitive to variations over their widths. Thus, the system's latency can be adjusted in exchange for a small reduction in the system's load. In case of having several tunnels, this load reduction only allows to tune the width of the narrowest tunnel, the one closest to the fixed point ξ_* associated with the interference level.

5.1 Further research topics

During the development of this work, some loose ends have been left dangling for future research. In the following lines, we enumerate the most promising topics that should be investigated:

(i) **Saturation point of the system.** We have shown that the optimum distribution of ordered energies yields a multi-uniform structure. However, the number of levels of such distribution remains unsolved for an arbitrary scenario parameters. In the simulations section, we obtained optimum profiles with $p = 5$ levels but more levels are expected for increasing loads. The saturation point of the system, characterized the number of levels that the optimum profile has and the traffic load at which this occurs, is still unknown.

(ii) **System's latency.** As stated at the end of Section 2.4.2, the proposed architecture presents latency issues especially in case of constricted tunnels. In the VC problem introduced in Section 3.2, we only address the limit situation in which $f(\xi)$ is bounded from above by the ξ line. From the authors' view, it seems interesting to see the deviation of the optimum level values, the change/collapse loads, and the throughput degradation when $f(\xi)$ is bounded from above by an ad-hoc function $g(\xi)$, so as to tune the tunnels apertures, and thus, the system's latency. Certainly, the identification of which $g(\xi)$ function is the most suitable is also a future research line.

(iii) **Mitigation of the imperfect cancellation effect.** As clarified at the end of Section 2.2, the proposed multistage DF structure allows improving the reconstruction of each user's signal throughout DF stages. In Chapter 4, we considered an imperfect cancellation function independent of the SINR. It would be convenient to evidence the effect of considering a real residual interference energy function in order to evaluate the gain in terms of throughput that is achieved when this DF architecture is implemented.

(iv) **Finite user evaluation of the asymptotic expressions.** As it has been shown during the document, we only address the case in which the number of users and the spreading gain tend to infinity. Naturally, this assumption is unrealistic, but it captures the essential features of a user-asymptotic scheme while simplifying the mathematical treatment. Hence, it is appropriate to evaluate from which number of users the finite user expressions start matching the user-asymptotic ones, similarly to [41] where the statement is verified for $K \geq 128$.

Appendix A

Acronyms

5G	Fifth Generation Wireless Systems
CC	Convolutional Code
CDMA	Code-Division-Multiple-Access
CRC	Cyclic Redundancy Check
D&R	Detector and Reconstructor
DF	Decision-Feedback
DS	Direct Sequence
DS-CDMA	Direct-Sequence Code-Division-Multiple-Access
EsNo	Energy per Symbol to Noise Power Spectral Density Ratio
FEC	Forward Error Correction
FLCV	Fundamental Lemma of the Calculus of Variations
FP	Fixed Point
IC	Interference Cancellation
IoT	Internet of Things
KKT	Karush-Khun-Tucker
LDPC	Low-Density Parity-Check
M2M	Machine To Machine

MA	Multiple Access
MAI	Multiple Access Interference
MLSE	Maximum Likelihood Sequence Estimator
MUD	Multiuser Detector
PER	Packet Error Rate
PSR	Packet Success Rate
PMDF	Parallel Multistage Decision-Feedback
QPSK	Quadrature Phase-Shift Keying
RA	Random Access
SIC	Successive Interference Cancellation
SINR	Signal-to-Interference-plus-Noise Ratio
SNR	Signal-to-Noise Ratio
SPE	Stationary Point Equation
TC	Transversality Condition
VC	Variational Calculus
WE	Weierstrass-Erdmann

Appendix B

Equivalence Between VC Problems

As described in Section 3.2, even when pursuing the aim of finding the optimum energy allocation function $E_{\mathrm{s}}(t)$ or $E_{\mathrm{r}}(t)$, it is convenient to transform the problem in terms of the SINR profile $\Gamma_*(t)$.

This annex comprises two parts. The first one is focused on proving the equivalence between both stated VC problems (3.4 - 3.7) and (3.13 - 3.15). The scope of the second section is to derive the equations that allow us to compute the energy profiles $E_{\mathrm{s}}(t)$ and $E_{\mathrm{r}}(t)$ once the optimum SINR profile $\Gamma_*(t)$ is found.

Equivalence between VC problems

Let us retrieve the previously presented VC problem in terms of the SINR profile (3.13 - 3.15),

$$\max_{\tau,\, \Gamma_*(t)} \quad \sum_{k=1}^{p} \int_{t_{k-1}}^{t_k} \mathrm{PSR}[\Gamma_*(t)]\, \mathrm{d}t \tag{B.1}$$

$$\text{s.t.} \quad \overline{\gamma} \;=\; \sum_{k=1}^{p} \int_{t_{k-1}}^{t_k} R(t, \Gamma_*(t))\, \mathrm{d}t \tag{B.2}$$

$$\text{s.t.} \quad 0 \;\geq\; \left(\sum_{k=1}^{p} \int_{t_{k-1}}^{t_k} R(t, x \cdot \Gamma_*(t))\, \mathrm{d}t \;-\; \overline{\gamma} \right) \qquad 0 < x < 1 \tag{B.3}$$

Using the relation $x = \frac{N_0+\xi_*}{N_0+\xi}$, the former problem can be converted, in terms of the received energy profile $E_{\mathrm{r}}(t)$, as follows,

$$\max_{\tau,\, E_{\mathrm{r}}(t)} \quad \sum_{k=1}^{p} \int_{t_{k-1}}^{t_k} \mathrm{PSR}\left[\frac{E_{\mathrm{r}}(t)}{N_0+\xi_*}\right] \mathrm{d}t \tag{B.4}$$

$$\text{s.t.} \quad \overline{\gamma} \;=\; \sum_{k=1}^{p} \int_{t_{k-1}}^{t_k} R\left(t, \frac{E_{\mathrm{r}}(t)}{N_0+\xi_*}\right) \mathrm{d}t \tag{B.5}$$

$$\text{s.t.} \quad 0 \;\geq\; \left(\sum_{k=1}^{p} \int_{t_{k-1}}^{t_k} R\left(t, \frac{E_{\mathrm{r}}(t)}{N_0+\xi}\right) \mathrm{d}t \;-\; \overline{\gamma} \right) \qquad \xi \;>\; \xi_* \tag{B.6}$$

where the set of constraints from $0 < x < 1$ is mapped onto $\xi > \xi_*$. At this point, it is clear that the problem evinces ambiguity in its resolution, since any pair $\{E_{\mathrm{r}}(t), \xi_*\}$ such that $\Gamma_*(t) = E_{\mathrm{r}}(t)/(N_0+\xi_*)$ is solution to the stated problem. This is due to the fact that we have combined the energy constraint (3.5) and the fixed point equation (3.6) to constitute a unique constraint in terms of the SINR profile $\Gamma_*(t)$.

This result highlights the fact that the solution in terms of $E_{\mathrm{r}}(t)$ requires an additional equation which can help us solve the present ambiguity. For instance, the energy constraint (3.5) or the fixed point equation (3.6) should be included. In both cases, the problem becomes equivalent to (3.4 - 3.7).

The intuitive idea behind this equivalence is that, in fact, as the involved functions PER[Γ] and $\epsilon(\Gamma)$ depend on Γ, the relevance lies in the SINR values of the optimal profile. In other words, the energy and MAI values are not important by themselves. What is crucial is their quotient through the SINR.

Computation of the energy profiles from the SINR profile

Let $\Gamma_*(t)$ be the optimum SINR profile obtained as the result of solving the VC problem (B.1 - B.3). We express the transmitted energy profile $E_{\mathrm{s}}(t)$ as a function of the SINR profile $\Gamma_*(t)$, as follows,

$$E_{\mathrm{s}}(t) \;=\; (N_0 + \xi_*)\frac{\Gamma_*(t)}{h(t)} \tag{B.7}$$

The reader should note that it is not possible to obtain directly $E_{\mathrm{s}}(t)$ from $\Gamma_*(t)$, given that both $\{E_{\mathrm{s}}(t), \xi_*\}$ are unknowns of the previous equation. In order to solve this ambiguity, we make use of the average energy constraint $\overline{E}$, resulting in,

$$E_{\mathrm{s}}(t) \;=\; \overline{E}\cdot\frac{\Gamma_*(t)/h(t)}{\int_0^{t_p}\Gamma_*(t)/h(t)\;\mathrm{d}t} \qquad E_{\mathrm{r}}(t) \;=\; \overline{E}\cdot\frac{\Gamma_*(t)}{\int_0^{t_p}\Gamma_*(t)/h(t)\;\mathrm{d}t} \tag{B.8}$$

Appendix C

Second Variation Analysis

This annex is included to continue the second variation analysis performed in Section 3.3.2. First, we recover the expressions of the second variation previously derived therein,

$$\delta J\Big|_{\text{2nd,SP}} = \frac{1}{2}\sum_{k=1}^{p}\left(\frac{\partial^2 F_k}{\partial \Gamma^2}\right)\int_{t_{k-1}}^{t_k} v_{\text{SP}}^2(t)\,\mathrm{d}t \tag{C.1}$$

$$\frac{\partial^2 F_k}{\partial \Gamma^2} = \text{PSR}''[\Gamma_*^k] + \alpha\overline{\gamma}\sum_{i=0}^{M}\lambda_i\cdot x_i^2\cdot\Phi''[x_i\cdot\Gamma_*^k] \tag{C.2}$$

where $v_{\text{SP}}(t)$ are defined by the set of admissible variations particularized at the stationary point, which comprises (3.23) evaluated at those positions where $\lambda(x)$ is active (i.e. $\boldsymbol{x}$),

$$\sum_{k=1}^{p}\boldsymbol{Q}_k\int_{t_{k-1}}^{t_k} v_{\text{SP}}(t)\,\mathrm{d}t = 0 \tag{C.3}$$

with $\boldsymbol{Q}_k \doteq Q_k(\boldsymbol{x})$ and $Q_k \doteq \partial R_k/\partial\Gamma$ introduced in order to simplify posterior computations. We seek a closed-form expression that helps us to ensure the negativeness of the derived second variation. Certainly, if the maximum of $\delta J|_{\text{2nd,SP}}$ is negative, then, $\delta J|_{\text{2nd,SP}} < 0$ for any not-null considered variation. Therefore, the following VC problem over the admissible variations $v(t)$ at the SP needs to be addressed,

$$\max_{v(t)}\left[\,\delta J\Big|_{\text{2nd,SP}} = \frac{1}{2}\sum_{k=1}^{p}\left(\frac{\partial^2 F_k}{\partial\Gamma^2}\right)\int_{t_{k-1}}^{t_k} v_{\text{SP}}^2(t)\,\mathrm{d}t\,\right] \tag{C.4}$$

$$\text{s.t.}\quad \mathbf{0} = \sum_{k=1}^{p}\boldsymbol{Q}_k\int_{t_{k-1}}^{t_k} v_{\text{SP}}(t)\,\mathrm{d}t \tag{C.5}$$

We define the functional $\mathcal{G}$ that includes (C.4) and incorporates (C.5) using the set of Lagrange multipliers $\boldsymbol{\beta} = [\beta_0, \beta_1, ..., \beta_M]^T$. As a different VC problem is formulated, new variations need to be contemplated. In particular, we consider infinitesimal first order variations $w(t)$ over $v_{\text{SP}}(t)$ as $v_{\text{SP}}(t) + w(t)$, and we derive the first variation of $\mathcal{G}$,

$$\mathcal{G}[v_{\text{SP}}(t)] \doteq \sum_{k=1}^{p}\int_{t_{k-1}}^{t_k}\left(\frac{1}{2}\frac{\partial^2 F_k}{\partial\Gamma^2}\,v_{\text{SP}}^2(t) - (\boldsymbol{\beta}^T\boldsymbol{Q}_k)\,v_{\text{SP}}(t)\right)\mathrm{d}t \tag{C.6}$$

$$\delta\mathcal{G}\Big|_{\text{1st}} = \sum_{k=1}^{p}\int_{t_{k-1}}^{t_k}\left(\frac{\partial^2 F_k}{\partial\Gamma^2}\,v_{\text{SP}}(t) - \boldsymbol{\beta}^T\boldsymbol{Q}_k\right)w(t)\,\mathrm{d}t \tag{C.7}$$

Following the rationales explained in Section (3.2.1), we use the FLCV to obtain the SPEs of the former problem. Consequently, the following $k = 1, ..., p$ equations must be accomplished,

$$\frac{\partial^2 F_k}{\partial \Gamma^2}\, v_{\mathrm{SP}}(t) \;=\; \boldsymbol{\beta}^T \boldsymbol{Q}_k \qquad t_{k-1} < t \leq t_k \tag{C.8}$$

Once again, as the previous SPE does only depend on $v_{\mathrm{SP}}(t)$, the p-step function, with levels $\boldsymbol{v} \doteq [v_1, ..., v_p]^T$ defined within the user intervals $\boldsymbol{\Delta t}_v \doteq [\Delta t_1, ..., \Delta t_p]^T$, is an extremal of the stated VC problem. Hence, substituting into (C.4), we have that,

$$\delta J\Big|_{\mathrm{2nd,SP,max}} \;=\; \frac{1}{2}\sum_{k=1}^{p}\left(\frac{\delta^2 F_k}{\delta \Gamma^2}\cdot \Delta t_k \cdot v_k^2\right) \tag{C.9}$$

$$\mathbf{0} \;=\; \sum_{k=1}^{p}(\boldsymbol{Q}_k \cdot \Delta t_k \cdot v_k) \tag{C.10}$$

Now, substituting (C.8) into (C.9) and using (C.10) we obtain $\delta J|_{\mathrm{2nd,SP,max}} = 0$, which is not a sufficient condition for ensuring that the multiuniform solution $\Gamma_*(t)$ is a local maximizer of $\overline{\mathrm{psr}}_*$, provided that this maximum is not achieved for the trivial case of $\boldsymbol{v} = \mathbf{0}$. In this case, the proof would be invalid owing to the fact that, by definition, the variations $v(t)$ over the SINR profile must be non-null.

We are going to evidence under which conditions $\boldsymbol{v} = \mathbf{0}$ is the unique solution that fulfils (C.10). In matrix form we have,

$$\begin{bmatrix} Q_1(x_0) & \cdots & Q_p(x_0) \\ Q_1(x_1) & \cdots & Q_p(x_1) \\ \vdots & \ddots & \vdots \\ Q_1(x_M) & \cdots & Q_p(x_M) \end{bmatrix} \begin{bmatrix} \Delta t_1 v_1 \\ \Delta t_2 v_2 \\ \vdots \\ \Delta t_p v_p \end{bmatrix} = \begin{bmatrix} 0 \\ 0 \\ \vdots \\ 0 \end{bmatrix} \tag{C.11}$$

which constitutes the linear system $\boldsymbol{Q} \cdot \boldsymbol{u} = \mathbf{0}$, with $\boldsymbol{Q}$ and $\boldsymbol{u}$ defined by context. It is easy to see that, given that $\boldsymbol{\Delta t}_v \neq \mathbf{0}$, $\boldsymbol{v} = \mathbf{0}$ is the unique solution of the previous linear system of equations if and only if $p \leq M + 1$ as long as $\boldsymbol{Q}$ is a non-singular matrix.

For the rest of the document, we will assume that this matrix is of full-rank, and thus, the derived inequality $p \leq M + 1$ is a sufficient condition for having a solution that does not correspond to a saddle point.

Concretely, we cannot be sure that the obtained extremal in (C.8) corresponds to a local maximum or minimum of (C.4 - C.5). Nonetheless, by taking the second variation of this problem, it can be proven that, in order to ensure its negativity a new VC problem equivalent to the one stated in (C.4 - C.5) is required. Due to the recursion of the problem, it can be proven that the solution is coherent under the initial assumption $\delta J|_{\mathrm{2nd,SP}} < 0$. Henceforth, in order to verify this assumption, we will only consider those solutions such that all terms in (C.2) are negative and the derived inequality is fulfilled.

Appendix D

Relationship with Previous Works

In this section, we relate the obtained mathematical expressions with previous works, mostly developed by the advisors of this thesis. In particular, we will focus our attention on [29], in which the authors derive the optimum energy allocation function of a massive uncoordinated spread-spectrum MA network when:

(i) Users share the same encoder with known PER curve and may limit their power transmissions according to an average energy constraint over the user population.

(ii) The receiver node implements a SIC strategy (of a single iteration) in order to mitigate MAI.

As in this work the authors only consider continuously differentiable ordered energy distributions over the user interval $0 \leq t \leq t_1 \leq 1$, we will center the subsequent comparison on the same case. Moreover, uniform and unitary channel gains are assumed.

We take the SPE in [29], denoted the *Invariance Equation*, as depicted below,

$$\rho \;=\; \frac{\mathrm{PSR}'[\Gamma_*(t)]}{N_t(t) \;-\; \alpha I(t)\Phi'[\Gamma_*(t)]} \tag{D.1}$$

with $I(t) \doteq \int_t^1 E_{\mathrm{r}}(\tau)\,\mathrm{d}\tau$ the integrated remaining energy profile and $N_t(t) = E_{\mathrm{s}}(t)/\Gamma(t)$ the noise plus interference term. In the following lines, we will compare the SPE of both IC schemes in order to assess whether the behaviour/performance of one of the schemes can be predicted from the other one,

$$\lambda(x_0) \;=\; \frac{\mathrm{PSR}'[\Gamma_*(t)]}{1 \;+\; \alpha\theta\overline{\gamma} \;-\; \alpha\overline{\gamma}\Phi'[\Gamma_*(t)]} \tag{D.2}$$

$$\rho \;=\; \frac{\mathrm{PSR}'[\Gamma_*(t)]}{N_t(t) \;-\; \alpha I(t)\Phi'[\Gamma_*(t)]} \tag{D.3}$$

As in can be seen, both equations present close similarities that we can relate with the fact that different IC strategies are considered. In our case study (parallel architecture), we have that, $\Gamma_*(t) = \Gamma_*$ is a solution of (D.2). Moreover, for the SIC case, if we take (D.3) for $t = 0$ we have that $I(0) = \overline{E}$ and $N_t(0) = N_0 + \alpha\theta\overline{E}$. Substituting into (D.3), we have that,

$$\lambda(x_0) \;=\; \frac{\mathrm{PSR}'[\Gamma_*]}{1 \;+\; \alpha\theta\overline{\gamma} \;-\; \alpha\overline{\gamma}\Phi'[\Gamma_*]} \tag{D.4}$$

$$\rho \;=\; \frac{\mathrm{PSR}'[\Gamma_*(0)]}{N_0 \;+\; \alpha\theta\overline{E} \;-\; \alpha\overline{E}\Phi'[\Gamma_*(0)]} \tag{D.5}$$

where both equations result equivalent if we divide at both sides of (D.5) by N_0.

It seems curious that two mathematics so distant turn into such similar equations. So far, it is just a coincidence that we shall study in depth to evidence whether there really exists an ulterior motive that would allow us to find a relationship between both policies.

The reader must be aware that this proof has only been obtained for the case of continuously differentiable functions. It remains unknown if for the discontinuous case there is such a tight relationship can also be found between the stationary point equations of both architectures.

However, no expression has been derived for the SIC receiver considering a broader space of functions. Thus, no further studies can be undertaken in this section.

Appendix E

PER Curves of the Considered FEC Codes

As it can be seen in the present work, not only the PER[Γ] and PSR[Γ] curves are important for the derived equations but also their derivatives with respect to the variable Γ. For the present reason, this section is dedicated to show the exact shape of the mentioned curves. We depict in Figure E.1 the PER[Γ] and PSR[Γ] curves for both described codes and in Figure E.2 their first and second derivatives.

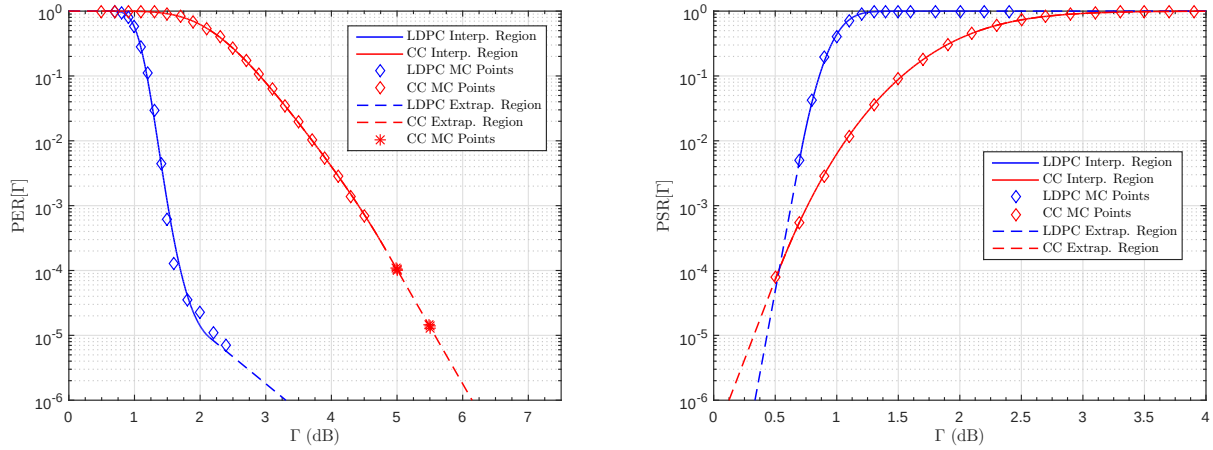

Figure E.1: PER[Γ] (left) and PSR[Γ] (right) curves of the LDPC (blue) and CC (red) codes.

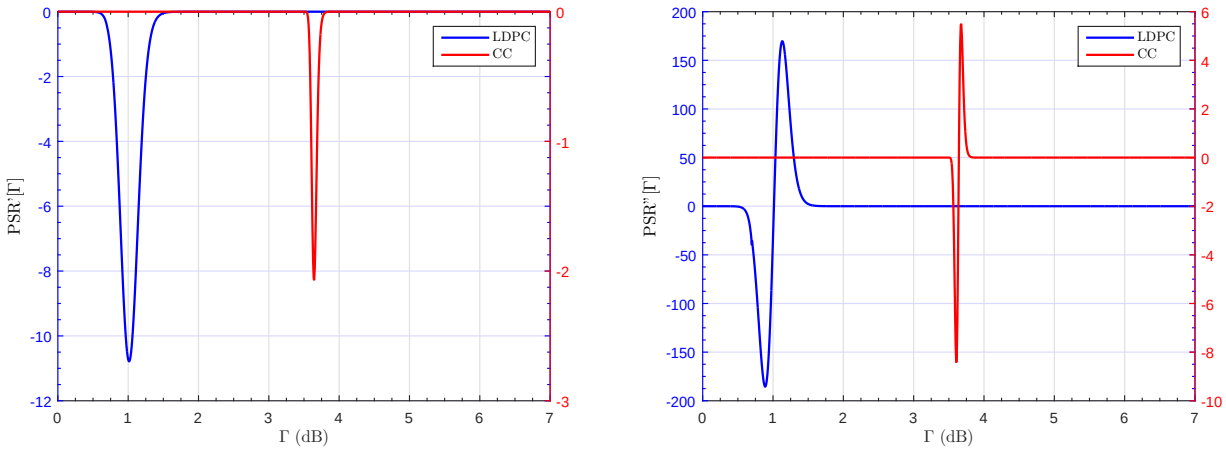

Figure E.2: PER′[Γ] (left) and PER″[Γ] (right) curves of the LDPC (blue) and CC (red) codes.

Results evidence the clean definition of both curves even near the inflexion point of both codes. It is important to remark that some numerical problems have been avoided as a matter of using those very well defined PER and PSR curves.

Appendix F

Correlator Bank

In this section, we derive the optimal SINR profile that maximizes the throughput of the network described in Chapter 2 when the receiver implements a conventional CDMA correlator bank. The resulting equations may be of interest in order to benchmark the benefit of the proposed IC scheme. For simplicity, we will only address the case of constant channel gains.

Optimization problem: The constant channel case

We take the stated VC problem in Section 3.2 and we particularize it for the case of no cancellation and for constant channel gains. Moreover, advancing the solution, we simplify the considered space up to continuously differentiable functions with a user admission index. Therefore, the following VC problem needs to be solved,

$$\max_{\tau,\,\Gamma(t)} \quad \left[\overline{\text{psr}} \;=\; \int_0^{t_1} \text{PSR}\left[\Gamma(t)\right]\,\mathrm{d}t \right] \tag{F.1}$$

$$\text{s.t.} \quad \overline{\gamma} \;=\; \int_0^{t_1} \Gamma(t)\left(1 \,+\, \alpha\theta\overline{\gamma}\right)\,\mathrm{d}t \tag{F.2}$$

We build the Lagrangian that incorporates the $\overline{\text{psr}}$ functional along the stated constraint through the Lagrange multiplier λ, as follows,

$$J[\Gamma(t)] \;\doteq\; \int_0^{t_1} \text{PSR}\left[\Gamma(t)\right]\,\mathrm{d}t \;-\; \lambda\left(\int_0^{t_1} \Gamma(t)\left(1 \,+\, \alpha\theta\overline{\gamma}\right)\,\mathrm{d}t \;-\; \overline{\gamma}\right) \tag{F.3}$$

We consider variations $v(t)$ over the SINR profile and free variations δt_1 over the end point t_1. We follow the development presented in Section 3.2.1 in order to derive the SPE of the former problem,

$$\rho \;=\; \text{PSR}'\left[\Gamma(t)\right] \qquad 0 < t \leq t_1 \tag{F.4}$$

again, as the SPE does only depend on $\Gamma(t)$, the uniform solution $\Gamma(t) = \overline{\Gamma}$ for $0 < t \leq t_1$ with $\overline{\Gamma} \doteq \overline{\gamma}/(1+\alpha\theta\overline{\gamma})$ is an extremal of the considered functional. Moreover, the TC at the end point t_1 results in,

$$\text{PSR}\left[\Gamma(t_1)\right] \;-\; \rho\cdot\Gamma(t_1) \;=\; 0 \tag{F.5}$$

Combining (F.4 - F.5) at the end point t_1, we have that,

$$\text{PSR}[\Gamma(t_1)] \;=\; \text{PSR}'[\Gamma(t_1)]\Gamma(t_1) \tag{F.6}$$

which only depends on the used FEC code through the previous non-linear equation.

Second variation analysis

We perform a second order expansion of the considered functional, and we particularize it at the stationary point, where the first variation vanishes and also may second order terms. Therefore, we obtain,

$$\delta J\big|_{\text{2nd,SP}} \;=\; \frac{1}{2}\cdot \text{PSR}''\left[\,\overline{\Gamma}\,\right]\int_0^{t_1} v^2(t)\,\text{d}t \tag{F.7}$$

A sufficient condition for ensuring that the uniform solution is a local-maximizer of $\overline{\text{psr}}$ is to set $\delta J\big|_{\text{2nd,SP}} < 0$, that must be verified regardless of any admissible variation $v(t)$ and δt_1. Thus, we have that $\Gamma(t) \geq \Gamma_{\text{ip}}$ for $0 \leq t \leq t_1$ with $\Gamma_{\text{ip}} \doteq \text{PSR}''^{-1}[0]$.

Solution procedure

In the following lines, we describe the main procedure performed in order to find the optimal SNIR profile.

1. Solve the non-linear equation (F.6) and keep only those candidates $\Gamma(t_1) \geq \Gamma_{\text{ip}}$.
2. Compute the end point t_1 as $t_1 \doteq \min\{1,\, \overline{\Gamma}/\Gamma(t_1)\}$.
3. Compute the optimum SINR profile as,

$$\Gamma(t) \;=\; \begin{cases} \max\{1,\, \overline{\Gamma}/\Gamma(t_1)\} & \text{for} \quad 0 < t \leq t_1 \\ \\ 0 & \text{for} \quad t_1 < t \leq 1 \end{cases} \tag{F.8}$$

Bibliography

[1] Izrail Moiseevitch Gelfand, Richard A Silverman, et al. *Calculus of Variations*. Courier Corporation, 2000.

[2] Zaher Dawy, Walid Saad, Arunabha Ghosh, Jeffrey G Andrews, and Elias Yaacoub. Toward Massive Machine Type Cellular Communications. *IEEE Wireless Communications*, 24(1):120–128, 2017.

[3] 5G Infrastructure PPP Association et al. 5G Vision-The 5G Infrastructure Public Private Partnership: The Next Generation of Communication Networks and Services. *White Paper, February*, 2015.

[4] Maria Rita Palattella, Mischa Dohler, Alfredo Grieco, Gianluca Rizzo, Johan Torsner, Thomas Engel, and Latif Ladid. Internet of Things in the 5G Era: Enablers, Architecture, and Business Models. *IEEE Journal on Selected Areas in Communications*, 34(3):510–527, 2016.

[5] Yang Cao, Tao Jiang, and Zhu Han. A Survey of Emerging M2M Systems: Context, Task, and Objective. *IEEE Internet of Things Journal*, 3(6):1246–1258, 2016.

[6] Mamta Agiwal, Abhishek Roy, and Navrati Saxena. Next Generation 5G Wireless Networks: A Comprehensive Survey. *IEEE Communications Surveys & Tutorials*, 18(3):1617–1655, 2016.

[7] Mohammad Islam, Abd-elhamid Taha, and Selim Akl. A Survey of Access Management Techniques in Machine Type Communications. *IEEE communications Magazine*, 52(4):74–81, 2014.

[8] Carsten Bockelmann, Nuno Pratas, Hosein Nikopour, Kelvin Au, Tommy Svensson, Cedomir Stefanovic, Petar Popovski, and Armin Dekorsy. Massive Machine-Type Communications in 5G: Physical and MAC-layer Solutions. *IEEE Communications Magazine*, 54(9):59–65, 2016.

[9] Oscar del Rio Herrero and Riccardo De Gaudenzi. Generalized Analytical Framework for the Performance Assessment of Slotted Random Access Protocols. *IEEE Transactions on Wireless Communications*, 13(2):809–821, 2014.

[10] Dimitri P Bertsekas, Robert G Gallager, and Pierre Humblet. *Data Networks*, volume 2. Prentice-Hall International New Jersey, 1992.

[11] Enrico Casini, Riccardo De Gaudenzi, and Oscar Del Rio Herrero. Contention Resolution Diversity Slotted ALOHA (CRDSA): An Enhanced Random Access Scheme for Satellite Access Packet Networks. *IEEE Transactions on Wireless Communications*, 6(4), 2007.

[12] Sergio Verdú and Shlomo Shamai. Spectral Efficiency of CDMA with Random Spreading. *IEEE Transactions on Information theory*, 45(2):622–640, 1999.

[13] Pierluigi Salvo Rossi, Kimmo Kansanen, Ralf R Müller, and Christoph Rachinger. Power Randomization for Iterative Detection Over Random-Access Fading Channels. *IEEE Transactions on Wireless Communications*, 14(10):5704–5713, 2015.

[14] Sergio Verdu. *Multiuser Detection*. Cambridge university press, 1998.

[15] Sergio Verdu. Minimum Probability of Error for Asynchronous Gaussian Multiple-Access Channels. *IEEE transactions on information theory*, 32(1):85–96, 1986.

[16] Sergio Verdú. Computational Complexity of Optimum Multiuser Detection. *Algorithmica*, 4(1):303–312, 1989.

[17] Russell Dodd, Christian Schlegel, and Vincent Gaudet. DS-CDMA Implementation with Iterative Multiple Access Interference Cancellation. *IEEE Transactions on Circuits and Systems I: Regular Papers*, 60(1):222–231, 2013.

[18] M Prabha and P Kumar. DS CDMA Multiuser Receiver Employing Multiple Access Interference Cancellation using Iterative Demodulator Architecture. In *Green Computing Communication and Electrical Engineering (ICGCCEE), 2014 International Conference on*, pages 1–5. IEEE, 2014.

[19] Pulin Patel and Jack Holtzman. Analysis of a Simple Successive Interference Cancellation Scheme in a DS/CDMA System. *IEEE journal on selected areas in communications*, 12(5):796–807, 1994.

[20] GS Deepthy and RJ Susan. Analysis of Successive Interference Cancellation in CDMA Systems. In *2012 Second International Conference on Advanced Computing & Communication Technologies*, pages 481–485. IEEE, 2012.

[21] Yingqun Yu and Georgios B. Giannakis. High-Throughput Random Access Using Successive Interference Cancellation in a Tree Algorithm. *IEEE Transactions on Information Theory*, 53(12):4628–4639, 2007.

[22] Adel Omar Dahmane and Lotfi Mejri. Block Decision Feedback Multistage PIC Scheme for DS-CDMA systems. In *2006 IEEE International Conference on Wireless and Mobile Computing, Networking and Communications*, pages 386–390. IEEE, 2006.

[23] Avneesh Agrawal, Jeffrey G Andrews, John M Cioffi, and Teresa Meng. Iterative Power Control for Imperfect Successive Interference Cancellation. *IEEE Transactions on wireless communications*, 4(3):878–884, 2005.

[24] Dejan V Djonin and Vijay K Bhargava. Asymptotic Analysis of the Conventional Decision Feedback Receiver in Fading Channels. *IEEE transactions on wireless communications*, 2(5):1066–1078, 2003.

[25] Dongning Guo and Sergio Verdú. Randomly Spread CDMA: Asymptotics Via Statistical Physics. *IEEE Transactions on Information Theory*, 51(6):1983–2010, 2005.

[26] Dongning Guo and Sergio Verdú. Replica Analysis of Large-System CDMA. In *Information Theory Workshop, 2003. Proceedings. 2003 IEEE*, pages 22–25. IEEE, 2003.

[27] Josep Sala-Alvarez, Javier Villares, and Francesc Rey. SINR Profile for Spectral Efficiency Optimization of SIC Receivers in the Many-User Regime. In *2015 IEEE International Conference on Communication Workshop (ICCW)*, pages 2063–2068. IEEE, 2015.

[28] Josep Sala, Francesc Rey, and Javier Villares. Asymptotically Optimum Energy Profile for Successive Interference Cancellation in DS-CDMA under a Power Unbalance Constraint. *IEEE communications letters*, 16(2):172–175, 2012.

[29] J. Sala Alvarez, F. Rey Micolau, Javier Villares, and Francesc Molina. Minimum PER User-Energy Profile for Massive SIC Receivers under an Average Energy Constraint. In *IEEE International Workshop on Signal Processing Advances for Wireless Communications*, pages 700 – 705, 2017 July.

[30] Husheng Li and H Vincent Poor. On Channel Capacity of Parallel Interference Cancellation with Outage Probability in Coded DS-CDMA Systems. In *Signals, Systems and Computers, 2004. Conference Record of the Thirty-Seventh Asilomar Conference on*, volume 1, pages 470–474. IEEE, 2003.

[31] Shimon Moshavi. Multi-User Detection for DS-CDMA Communications. *IEEE communications magazine*, 34(10):124–136, 1996.

[32] Y Bar-Ness and NJM Van Waes. Multistage Detect for Adaptive Separation of QAM-modulated Multiuser CDMA Signals. In *Spread Spectrum Techniques and Applications, 1998. Proceedings., 1998 IEEE 5th International Symposium on*, volume 3, pages 927–931. IEEE, 1998.

[33] Abdulkadir Dinc and Yeheskel Bar-Ness. Bootstrap: A Fast Blind Adaptive Signal Separator. In *Acoustics, Speech, and Signal Processing, 1992. ICASSP-92., 1992 IEEE International Conference on*, volume 2, pages 325–328. IEEE, 1992.

[34] Javier Villares, Francesc Rey, and Josep Sala-Alvarez. Optimum Energy Allocation for Massive Spread-Spectrum Multiple Access in Networks of Uncoordinated Energy-Limited Terminals. In *Signal Processing Advances in Wireless Communications (SPAWC), 2016 IEEE 17th International Workshop on*, pages 1–6. IEEE, 2016.

[35] John G Proakis. *Companders*. Wiley Online Library, 2001.

[36] R Michael Buehrer. Equal BER Performance in Linear Successive Interference Cancellation for CDMA Systems. *IEEE Transactions on Communications*, 49(7):1250–1258, 2001.

[37] Igor Griva, Stephen G Nash, and Ariela Sofer. *Linear and Nonlinear Optimization*. Siam, 2009.

[38] EN DVB. 300 421 v1. 1.2 (1997-08). *European Standard (Telecommu nications series)*.

[39] IEEE Computer Society LAN MAN Standards Committee et al. Wireless LAN Medium Access Control (MAC) and Physical Layer (PHY) Specifications. *IEEE Standard 802.11-1997*, 1997.

[40] EN ETSI. 302 307 v1. 2.1 (2009-08). *Digital Video Broadcasting (DVB)*, 2009.

[41] Josep Sala, Javier Villares, and Francesc Rey. Asymptotic and Finite User PER Analysis of Successive Interference Cancellation for DS-CDMA. *IEEE communications letters*, 15(11):1145–1147, 2011.